Journal Pre-proof

Dapagliflozin Attenuates Diabetes-Induced Podocyte Lipotoxicity via ERRα-Mediated Lipid Metabolism

Hongtu Hu, Juan Wang, Zhuan Peng, Yanqin Fan, Qian Yang, Jijia Hu

PII: S0891-5849(25)00238-2

DOI: https://doi.org/10.1016/j.freeradbiomed.2025.04.028

Reference: FRB 17053

To appear in: *Free Radical Biology and Medicine*

Received Date: 7 March 2025

Revised Date: 27 March 2025

Accepted Date: 18 April 2025

Please cite this article as: H. Hu, J. Wang, Z. Peng, Y. Fan, Q. Yang, J. Hu, Dapagliflozin Attenuates Diabetes-Induced Podocyte Lipotoxicity via ERRα-Mediated Lipid Metabolism, *Free Radical Biology and Medicine*, https://doi.org/10.1016/j.freeradbiomed.2025.04.028.

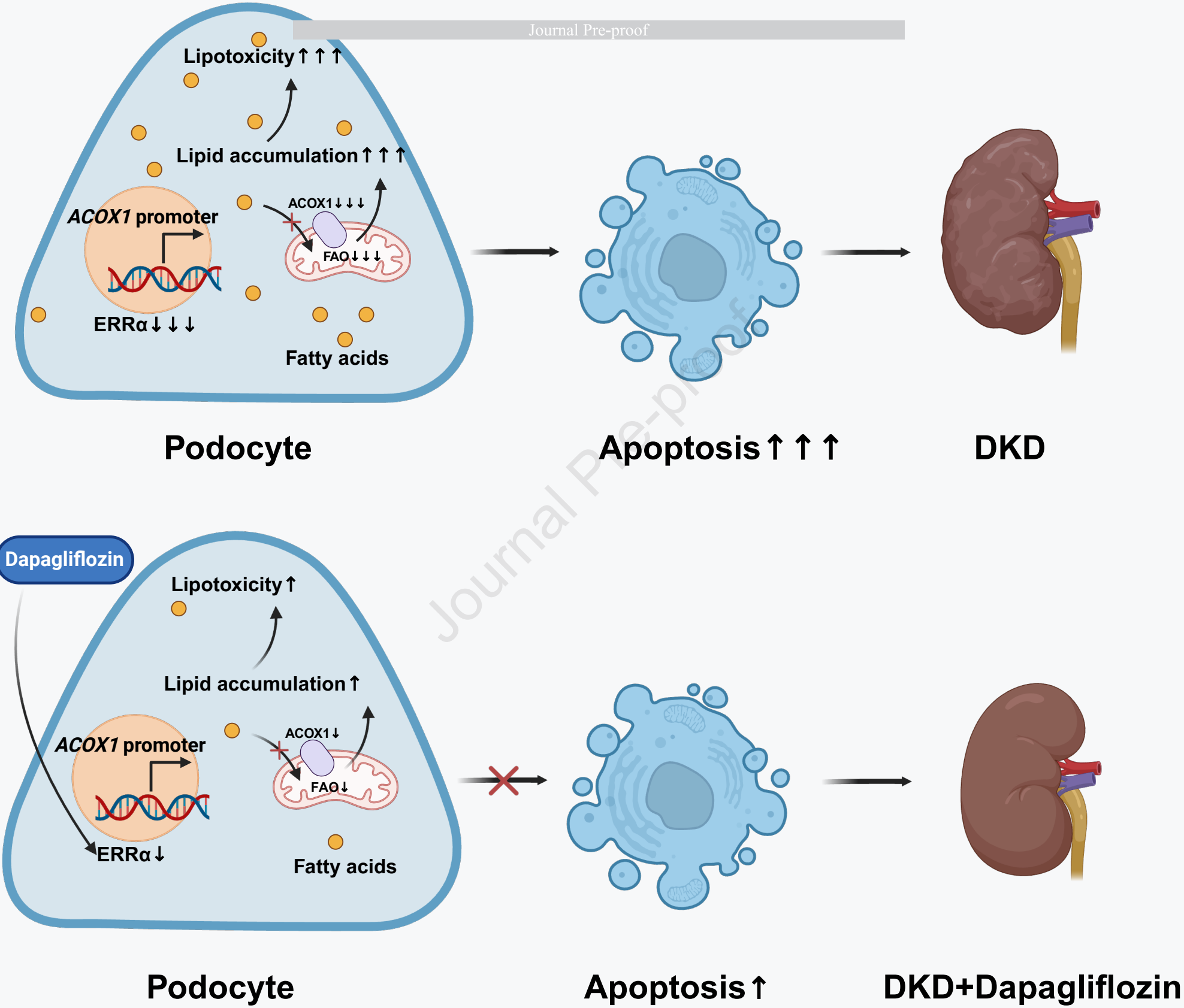

Dapagliflozin Attenuates Diabetes-Induced Podocyte Lipotoxicity via ERRα-Mediated Lipid Metabolism

Hongtu Hu[1,†], Juan Wang[1,†], Zhuan Peng[1], Yanqin Fan[1], Qian Yang[1], Jijia Hu[1,*]

[1]Division of Nephrology, Renmin Hospital of Wuhan University, Wuhan, China; Nephrology and Urology Research Institute of Wuhan University, Wuhan, China

[†]Hongtu Hu and Juan Wang contributed equally to this work

*Correspondence author

Email: hujijia@whu.edu.cn (J.Hu)

ABSTRACT

Diabetic kidney disease (DKD) is a major complication of diabetes mellitus, characterized by podocyte injury and lipid accumulation, which contribute to high morbidity and mortality. Current treatments primarily alleviate symptoms, underscoring the need for targeted therapies to address the underlying mechanisms of DKD progression. This study explores the protective effects of dapagliflozin (DAPA), a selective sodium-glucose cotransporter 2 (SGLT2) inhibitor, on podocyte lipotoxicity and its regulatory role in the estrogen-related receptor alpha (ERRα)-acyl-CoA oxidase 1 (ACOX1) axis. Using db/db mice and streptozotocin-induced DKD models, we demonstrate that DAPA significantly reduces the urinary albumin-to-creatinine ratio (ACR) and improves renal pathology by alleviating glomerular hypertrophy, mesangial matrix expansion, and podocyte foot process effacement. DAPA also decreases triglyceride and free fatty acid accumulation in glomeruli, as evidenced by Oil Red O and BODIPY staining. Mechanistically, DAPA upregulates ERRα and ACOX1 expression in podocytes, enhancing fatty acid oxidation (FAO) and mitigating lipidtoxicity. Loss of ERRα exacerbates lipid-induced podocyte injury, while ERRα overexpression confers protective effects. These findings highlight DAPA's renoprotective effects via modulation of the ERRα-ACOX1 axis, suggesting that targeting ERRα could be a promising therapeutic strategy for DKD.

Keywords

Diabetic Kidney Disease, Dapagliflozin, Podocytes, Lipotoxicity, ERRα, Fatty Acid Oxidation

31 **Abbreviations:**

32 ACOX1, Acyl-CoA oxidase 1; ACR, Albumin to Creatinine Ratio; ATP, Adenosine Triphosphate;
33 BSA, Bovine Serum Albumin; BUN, Blood Urea Nitrogen; ChIP-seq, Chromatin
34 Immunoprecipitation Sequencing; CCK-8, Cell Counting Kit-8; Cr, Creatinine; DAPA, Dapagliflozin;
35 DKD, Diabetic Kidney Disease; ERRα, Estrogen-related receptor alpha; FFA, Free Fatty Acid; FITC,
36 Fluorescein Isothiocyanate; HRP, Horseradish Peroxidase; IHC, Immunohistochemistry; IF,
37 Immunofluorescence; ITS, Insulin-Transferrin-Selenium; LUC, Luciferase; NPHS2, Nephrosis 2;
38 OCR, Oxygen Consumption Rate; ORO, Oil Red O; PAS, Periodic Acid-Schiff; PE, Phycoerythrin;
39 qRT-PCR, Quantitative Real-Time Polymerase Chain Reaction; SDS-PAGE, Sodium Dodecyl
40 Sulfate-Polyacrylamide Gel Electrophoresis; SGLT2, Sodium-glucose co-transporter-2; STZ,
41 Streptozotocin; TEM, Transmission Electron Microscopy; TG, Triglyceride; WB, Western Blot
42

Background

Diabetic kidney disease (DKD), also known as diabetic nephropathy, is a common and severe complication of diabetes mellitus (DM)[1]. Altered lipid metabolism, including genes involved in fatty acid oxidation (FAO) and oxidative phosphorylation (OXPHOS) in kidney cells, is significantly correlated with the progression of DKD[2, 3]. Podocyte injury plays a pivotal role in the pathogenesis of DKD. Damage and loss of podocytes disrupt the normal structure of the glomerular basement membrane, directly leading to proteinuria. Recently, our group and others have reported that lipid deposition in podocytes is associated with glomerulosclerosis and proteinuria[4-6]. Growing evidence suggests that dysregulation of β-oxidation and intracellular lipid trafficking contributes to podocyte dysfunction and apoptosis, a condition known as lipotoxicity[7]. Attenuating renal lipid accumulation can improve podocyte damage and delay renal function decline[8]. However, clinical studies have shown that the use of statins to correct hyperlipidemia does not prevent the progression to end-stage renal disease (ESRD)[9]. Therefore, exploring effective therapeutic targets to improve podocyte lipid metabolism in DKD is crucial.

Dapagliflozin (DAPA), a selective inhibitor of sodium-glucose transport protein 2 (SGLT2), lowers blood glucose by blocking glucose reabsorption in the renal proximal tubule and stimulating urinary glucose excretion without inducing an increase in insulin release[10]. Several large-scale clinical trials, such as EMPA-REG OUTCOME, CREDENCE, and DAPA-CKD, have investigated the impact of SGLT2 inhibitors on renal outcomes[11, 12]. DAPA significantly reduced renal events in these studies and exhibited renal protective effects in diabetic patients. Thus, DAPA is considered a novel pharmacological alternative for counteracting the progression of DKD[13]. Intriguingly, DAPA also exhibits a renoprotective effect by improving renal lipid metabolism[14]. Recent investigations have demonstrated that SGLT2 inhibitors decrease podocyte cholesterol accumulation,

suggesting that DAPA protects the kidney through pleiotropic effects beyond glycemic control[15, 16]. However, the underlying molecular mechanisms by which DAPA influences podocyte fatty acid (FA) metabolism remain unclear.

Peroxisomal acyl-coenzyme A oxidases (ACOXs) are the initial and rate-limiting enzymes that catalyze the β-oxidation system in mitochondria[17]. ACOXs are generally classified into three subtypes: ACOX1, ACOX2, and ACOX3. Studies have shown that ACOXs are essential for renal FAO and redox homeostasis[18, 19]. ACOX polymorphisms are associated with DM, suggesting that ACOXs may be crucial for modulating lipid metabolism disorders in DKD[20]. Moreover, differential expression of ACOX1 in podocytes under high glucose stimulation has been reported[21]. ACOX1 deficiency leads to lipid accumulation and impaired FAO in the kidney, whereas upregulation of ACOX1 expression can improve renal metabolism and delay renal fibrosis in DKD[21, 22]. Additionally, emerging studies have shown that DAPA regulates lipid biosynthesis and degrading protein levels[23]. Researchers have reported that treating Zucker diabetic fatty (ZDF) rats with DAPA reduced hepatic lipid accumulation by upregulating ACOX1[24]. However, the mechanism by which DAPA regulates podocyte ACOX1 expression and lipotoxicity in DKD remains unclear.

Estrogen-related receptor α (ERRα) is a nuclear receptor with essential metabolic regulatory functions[25-27]. ERRα depletion has been identified to cause mitochondrial dysfunction, leading to cell death[28]. Increasing evidence indicates that ERRα may be an emerging target for regulating renal FAO and OXPHOS[29]. Furthermore, estrogen-related receptor agonism has been found to reverse mitochondrial dysfunction in the aging kidney, suggesting that ERRα may be a key target for improving podocyte lipid metabolism[30]. Available data suggest that ERRα is a transcriptional regulator of human ACOXs, activation of the ERRα-associated pathway decreases lipid deposition in

88 muscle cells by regulating the expression of genes related to FAO and OXPHOS[31]. Therefore, we
89 hypothesize that ERRα may play a critical role in regulating lipid metabolism in diabetic podocytes,
90 thereby contributing to the protective effect of SGLT2 inhibitors[30, 32].

91 In this study, we report that ERRα affects FAO in podocytes by regulating ACOX1 transcription.
92 The ERRα-ACOX1 axis is down-regulated in the DKD state, exacerbating lipotoxicity. Furthermore,
93 DAPA slows DKD progression by improving lipid metabolism and attenuating lipotoxicity by
94 activating the ERRα-ACOX1 axis, providing a potential therapeutic target for DKD.

95

Methods

Mice studies

All mice used in this study were maintained under specific pathogen-free (SPF) conditions, with humidity levels between 40% and 70%, temperatures ranging from 20 to 25°C, and a 12-hour light/12-hour dark cycle. They had unrestricted access to food and water. After the study, all mice were euthanized via an intraperitoneal injection of 150 mg/kg sodium pentobarbital. The kidneys were harvested for subsequent experiments. Each experiment involved at least six mice. All animal experimental procedures were conducted by the National Institutes of Health (NIH) Guidelines for the Care and Use of Laboratory Animals (Revised 2011), and ethical approval was obtained from the Ethics Committee for the Use of Animals of Wuhan University Renmin's Hospital (WDRM-2022397).

Establishment of animal models of DKD and drug treatment

Two DKD animal models were used in this study. The first model involved 8-week-old male db/db mice (genetic background of BKS), leptin-deficient, spontaneously obese diabetic mice that develop renal impairment (proteinuria, elevated blood creatinine, etc.). The second model was a streptozotocin (STZ)-induced DKD model. As previously reported, 8-week-old male $ERR\alpha^{podKI}/ERR\alpha^{ctrl}$ mice were administered STZ at 50 mg/kg via intraperitoneal injection for three consecutive days, followed by a high-fat diet[33]. After establishing the DKD model, dapagliflozin (DAPA, 1.0 mg/kg) or equivalent saline (VEH) was administered intraperitoneally daily for 4 weeks.

Establishment of $ERR\alpha^{podKI}$ mice

118 ERRα$^{flox/flox}$ knock-in mice (ERRα^{podKI}) (C57BL/6N background) were obtained from Cytogenes
119 Biosciences (Suzhou, China). Using the CRISPR/Cas9 system, we designed a pCAG-loxP-STOP-
120 loxP-ERRα construct containing the pCAG promoter, ERRα coding sequence, and a floxed STOP
121 cassette to regulate transcriptional activation. This construct was microinjected into fertilized zygotes,
122 targeting the male pronucleus. Recombinant transgenic offspring were generated through Cre-
123 mediated recombination driven by NPHS2-Cre expression (Catalog #: 008205, Jackson Laboratory,
124 USA)[34]. The F1 progeny exhibited targeted ERRα expression, and their generation and validation
125 were conducted under blinded conditions.

126

127 **Intrarenal adeno-associated virus (AAV) delivery**

128 *In vivo*, the knockdown of ACOX1 was achieved by intrarenal AAV injection, as described
129 previously[35]. Four weeks before STZ treatment, 1×10^{12} genomic particles of AAV-nphs1-
130 shACOX1 (AAV-shACOX1) or AAV-nphs1-null (AAV-shNC) (WZBio, China) were delivered into
131 the kidney via in situ injection at six independent points.

132

133 **Isolation of glomeruli**

134 In brief, the digested mouse kidney tissue was sequentially passed through a 100-micron cell
135 strainer, a 70-micron cell strainer and a 40-micron cell strainer. Subsequently, the glomeruli are
136 harvested by washing the inner layer of the 40-micron screen with an equilibration buffer[35]. The
137 cell suspension is then subjected to centrifugation at 1500 rpm for a period of 5 minutes at a
138 temperature of 4°C, after which it is resuspended in 5 mL of culture medium.

139

140 **Cell line and treatment**

141 The immortalized human podocytes were provided by professor Moin A. Saleem from the
142 Academic Nephrology Department at Southmead Hospital, Bristol, UK [35, 36]. The podocytes were
143 cultured at 33°C in RPMI 1640 medium (HyClone, USA) supplemented with 10% heat-inactivated
144 fetal bovine serum (FBS, Sigma, USA), 100 U/mL penicillin-streptomycin (Invitrogen, USA), and
145 1× insulin-transferrin-selenium (ITS, Invitrogen, USA). The cells were incubated at 37°C for two
146 weeks to induce differentiation. The differentiated podocytes were then stimulated for 24 hours with
147 30 mM glucose or a hypertonic control (30 mM mannitol). For treatments involving overexpression
148 of ERRα and ACOX1, 2 μg of the human ERRα and ACOX1 overexpression plasmid or pcDNA3
149 was transfected into podocytes for 24 hours using X-tremeGENE HP Reagent (Roche, Germany). For
150 *in vitro* experiments with DAPA, 10 μM DAPA (MCE, USA) was used following 48 hours of
151 stimulation. Each experiment was validated using three independent podocyte clones.

152

153 **Human Kidney Biopsy Samples**

154 Kidney samples from DKD patients with confirmed clinical and pathological diagnoses were
155 obtained for this study. Detailed clinical data for the two patient groups, which were extracted by
156 researchers from medical records, are presented in Supplementary Table 1. This study was approved
157 by the Ethics Committee of Renmin Hospital of Wuhan University, and participants who provided
158 informed consent (WDRY2021-KS034) were granted access to digital medical records.

159

160 **Measurement of renal function parameters in mice**

161 Before euthanasia, 24-hour urine samples were collected from the mice using metabolic cages.
162 Blood samples were obtained via retro-orbital bleeding. Serum was separated by centrifugation using
163 an automated biochemical analyzer (Beckman, USA) to measure serum creatinine (Cr) and blood
164 urea nitrogen (BUN) levels. Urine sample supernatants were centrifuged and analyzed using an
165 ELISA kit (Abcam, USA) to quantify urine albumin levels. The urinary albumin-to-creatinine ratio
166 (ACR) was calculated from the urinary and creatinine levels.

167

168 **Cell viability assay**

169 The impact of elevated glucose levels and the influence of DAPA on podocyte viability were
170 evaluated using the Cell Counting Kit-8 (CCK-8; Beyotime, China). Briefly, cells were treated with
171 different conditions: 10 μL of CCK-8 solution was added to each well, and the cells were incubated
172 at 37°C for one hour in a 5% CO_2 incubator. Absorbance was measured at 450 nm using a fully
173 automated microplate reader (Thermo Scientific, USA).

174

175 **Histological and immunohistochemical staining**

176 Kidney tissues from DKD patients and animal models were sectioned, deparaffinized, hydrated,
177 and subjected to antigen retrieval. Periodic acid-Schiff (PAS) staining, BODIPY staining (Thermo
178 Scientific, USA), and Oil Red O (ORO) staining (Beyotime, China) were performed to observe
179 histopathological changes in the kidney. The average values of mesangial matrix expansion for PAS
180 staining and the area of positive staining for BODIPY/ORO were evaluated in each group using 30
181 randomly selected non-overlapping fields (Five visual fields for each section analyzed).

182 For immunohistochemistry (IHC), kidney sections were incubated with 5% bovine serum
183 albumin (BSA) for one hour at room temperature, followed by incubation with the primary antibody

overnight at 4°C. Subsequently, sections were incubated with horseradish peroxidase (HRP)-conjugated secondary antibody for one hour at room temperature, and immunoreactivity was detected using diaminobenzidine as the substrate. The primary antibodies used were ERRα (GTX108166, Genetex, USA) and ACOX1 (GTX32989, Genetex, USA). Positive areas or integrated optical density (IOD) were evaluated in each group using 30 randomly selected non-overlapping fields (Five visual fields for each section analyzed). Microscopic images were captured using an upright microscope (Olympus, Japan).

Immunofluorescence (IF) assay

Mouse kidney sections and cell cultures underwent pre-treatment as previously described for IF analysis. Sections were blocked with 5% BSA for one hour at room temperature. Subsequently, kidney sections or cell cultures were incubated with primary antibodies overnight at 4°C, followed by incubation with HRP-conjugated secondary antibodies at room temperature for one hour. The primary antibodies used were ERRα (GTX108166, Genetex, USA), ACOX1 (GTX32989, Genetex, USA), TFAM (ab119684, Abcam) and WT1 (ab89901, Abcam). Cell nuclei were stained using an anti-fluorescence quenching sealer containing DAPI (Thermo Scientific, USA). Intracellular lipid droplets were labeled using fluorescent probes BODIPY and ORO dye. Microscopic images were captured using a confocal microscope (Olympus, Japan). The average fluorescence intensity, mitochondrial morphology values were assessed by analyzing 15 randomly selected, non-overlapping fields in each group (Five visual fields for each section analyzed).

Adenosine triphosphate (ATP) analysis

ATP levels in the treated podocytes were quantified using an ATP assay kit (Beyotime, China).

207 Absorbance was measured using a fully automated enzyme label reader (Thermo Scientific, USA).

208

209 **Oxygen consumption rate (OCR) measurements**

210 The mitochondrial oxygen consumption rate (OCR) and extracellular acidification rate (ECAR)
211 were quantified using the XFe96 extracellular flux analyzer (Seahorse Bioscience, USA), following
212 the manufacturer's protocol. Briefly, cells were seeded in XF 24-well cell culture microplates, and
213 OCR was measured after sequential additions of oligomycin, FCCP, fisetinone, and antimycin A.

214

215 **Transmission electron microscopy (TEM)**

216 Kidney and podocyte samples were fixed, embedded in epoxy resin, and sectioned for TEM
217 analysis. As previously described[35], the glomerular foot process and podocyte mitochondrial
218 morphology were observed using a transmission electron microscope (Hitachi, Japan). Five fields of
219 view per sample were analyzed to calculate the glomerular foot process width and the proportion of
220 damaged podocyte mitochondria.

221

222 **Western blot (WB)**

223 Cells or isolated glomeruli were subjected to protein extraction and concentration determination.
224 Equal amounts of protein were loaded onto SDS-PAGE gels and transferred to PVDF membranes
225 (Millipore, USA). Membranes were blocked with Rapid Closure Buffer (Proteintech, China) for one
226 hour at room temperature, followed by overnight incubation with primary antibodies at 4°C. The
227 primary antibodies used were ERRα (GTX108166, Genetex, USA), ACOX1 (GTX32989, Genetex,
228 USA), and β-actin (ab8226, Abcam, UK). Membranes were then incubated with HRP-conjugated
229 secondary antibodies for one hour at room temperature and visualized using a chemiluminescent ECL

230 substrate (Abbkine, China). Bands were observed using an imaging system (Monad, China), and grey
231 values were quantified using ImageJ software.
232
233 **Apoptosis detection**
234 Apoptosis in cultured podocytes was assessed by flow cytometry using Annexin V-FITC and 7-
235 AAD double staining, following the manufacturer's instructions (FITC-Annexin V Apoptosis
236 Detection Kit with PE, BioLegend, USA). Briefly, podocytes were harvested, washed with cold PBS,
237 and resuspended in binding buffer. Cells were then incubated with Annexin V-FITC and PE at room
238 temperature in the dark before immediate analysis by flow cytometry to distinguish viable, early
239 apoptotic, and late apoptotic/necrotic cells. Proper controls were included to ensure accurate gating
240 and analysis.
241
242 **Determination of triglyceride (TG) and free fatty acid (FFA) concentrations**
243 According to the manufacturer's instructions, TG and FFA levels in mouse glomeruli and
244 podocytes were quantified using TG content kits (Beyotime, China) and FFA content kits (Sigma,
245 USA).
246
247 **Luciferase (LUC) Reporter Assay**
248 The LUC reporter assay was performed by Genecreate Bioscience (China). A target sequence
249 (wild-type or mutant) of approximately 200 base pairs from the ACOX1 gene promoter region was
250 inserted into the pGL3-basic plasmid. The ERRα coding sequence was inserted into the pcDNA3
251 plasmid. 293T cells were transfected with these plasmids, and LUC activity was measured using a
252 luminometer (Promega, USA) with a LUC assay kit (Yeasen, China).

253

254 **Quantitative reverse transcription-polymerase chain reaction (QRT-PCR) analysis**

255 Total RNA from mouse glomeruli was isolated using TRIzol reagent (Invitrogen, USA) and
256 reverse transcribed into cDNA. To detect mRNA expression levels, qRT-PCR was performed using a
257 real-time PCR system (Bio-Rad, USA). The primers used are detailed in Supplementary Table 2.

258

259 **RNA-sequencing (RNA-seq) and single-cell (sc) RNA-seq data analyses**

260 The GSE166239 dataset was retrieved from the GEO database and analyzed using an online
261 platform (bioinformatics.com.cn) for data processing and visualization. Differentially expressed
262 genes (DEGs) were identified through the DESeq2 algorithm with a significance threshold of $p <$
263 0.05. To compare gene expression across different groups, heatmaps were generated. Volcano plots
264 were used to highlight genes with *p*-values below 0.05 and a log2 fold change greater than 5,
265 indicating upregulation or downregulation. A correlation heatmap was created to examine gene
266 relationships, while a chord diagram was employed to explore key pathways related to DKD.

267 For single-cell RNA sequencing (scRNA-seq), the KIT website (humphreyslab.com/SingleCell/)
268 or the GEO database (GSE220939) was used for data analysis. The Uniform Manifold Approximation
269 and Projection (UMAP) algorithm helped visualize distinct renal cell clusters in the scRNA-seq data.
270 Most of the analysis scripts were written in Python and R, with the code available on the KIT website.

271

272 **Statistical analysis**

273 Quantitative data were expressed as the mean ± SD. Statistical analysis was performed using
274 GraphPad Prism 9.0 software (USA). Comparisons between two groups were made using the t-test,
275 while one-way ANOVA and Tukey's multiple comparisons test were used to compare more than two

groups. Each experiment was repeated at least three times. Bivariate correlation analysis was performed using Pearson's correlation. A *p*-value of less than 0.05 was considered statistically significant.

Results

Effects of DAPA on diabetes-induced glomerular lipid accumulation

To elucidate the effect of Dapagliflozin (DAPA) on glomerular lipid metabolism, db/db mice, a well-established insulin resistance diabetic model with progressive kidney injury, were treated with DAPA, and renal tissues were collected for further analysis (Figure 1A). Consistent with previous studies[37, 38], urinalysis revealed a significantly elevated urinary albumin-to-creatinine ratio (ACR) in db/db mice at the end of the observation period. In contrast, ACR was significantly reduced in DAPA-treated db/db mice compared to vehicle control (VEH)-treated mice (Figure 1B). Morphological changes were observed using periodic acid-Schiff (PAS) staining and transmission electron microscopy (TEM). PAS staining revealed glomerular hypertrophy, dilated mesangial matrix, and glycogen deposition in db/db mice (Figure 1C-D). TEM examination disclosed massive foot process effacement of the podocytes in db/db mice (Figure 1E). After DAPA treatment showed improvements in these pathological phenomena (Figure 1C-E). Additionally, we have also found that both triglyceride (TG) and free fatty acid (FFA) levels were elevated in the glomeruli of db/db mice compared to db/m mice (Figure 1F-G). Oil Red O staining (Figure 1H-I) and BODIPY staining (Figure 1J-K) consistently indicated that DAPA effectively inhibited renal lipid accumulation in diabetic mice.

Effects of DAPA on the expression of ERRα and ACOX1

Given that triglycerides are the main components of lipid droplets and that lipid accumulation results from an imbalance between triglyceride synthesis and clearance, we investigated pathways regulating glomerular triglyceride metabolism by analyzing the publicly available GEO database (GSE166239). As shown in Figure 2A, FA metabolism significantly differed between healthy controls

303 and DKD patient groups. Differential gene expression analysis revealed that ACOX1, a rate-limiting
304 enzyme in mitochondrial FAO, was downregulated in the glomeruli of DKD patients (Figure 2B).
305 Furthermore, ACOX1 expression was positively correlated with the estimated glomerular filtration
306 rate (eGFR) in DKD patients (Figure 2C). Our previous study demonstrated that the nuclear receptor
307 ERRα plays a distinct role in regulating renal FAO and OXPHOS [39, 40], further correlation analyses
308 showed that ERRα expression was positively correlated with eGFR in DKD patients (Figure 2D).
309 Single-cell RNA (GEO ID: GSE220939), transcriptome sequencing (GEO ID: GSE166239) and
310 Nephroseq (https://www.nephroseq.org/) data identified key genes related to fatty acid metabolism in
311 DKD development[41, 42]. Secondary analysis showed that ACOX1 expression was significantly
312 downregulated in podocytes of DKD patients, while pretreatment with DAPA upregulated ACOX1
313 expression (Figure 2E). We further assessed the expression of ERRα and ACOX1 in renal tissues.
314 Immunohistochemical staining revealed decreased expression of ERRα and ACOX1 in the glomeruli
315 of DKD patients and db/db mice. In contrast, DAPA significantly upregulated ERRα and ACOX1, as
316 evidenced by immunofluorescence co-staining in podocytes (Figure 2F-H). Western blot analysis of
317 isolated mouse glomeruli confirmed that DAPA partially reversed the diabetes-induced
318 downregulation of ERRα and ACOX1 in db/db mice (Figure 2I). These results suggest that decreased
319 expression of ERRα and ACOX1 may be key indicators of dysregulated glomerular lipid metabolism
320 in DKD and that DAPA may alleviate renal lipid accumulation by upregulating ERRα and ACOX1
321 expression.
322

323 **DAPA treatment mitigates high glucose-induced lipid accumulation in vitro**

324 To investigate the role of DAPA in lipid metabolism, an *in vitro* high glucose (HG)-induced
325 human podocyte model was established. A cell viability assay (CCK8) was first employed to ascertain

326 the impact of HG and DAPA concentrations on cellular viability (Figure S1A-B). The findings
327 indicated that a 30 mM HG concentration did not significantly affect cell viability, whereas a 10 mM
328 DAPA concentration notably mitigated the impaired cell viability. Lipid accumulation in podocytes
329 was examined using Oil Red O (ORO) and BODIPY staining (Figure 3A-B). Lipid droplets were
330 detected in podocytes stimulated with HG, but pre-treatment with DAPA reduced lipid deposition.
331 Intracellular free fatty acids (FFA) and triglycerides (TG) were also assayed (Figure 3C-D), revealing
332 that DAPA treatment alleviated the increased FFA and TG content induced by HG.

333 Moreover, HG increased cellular apoptosis, but DAPA diminished this cellular damage (Figure
334 3E). As cellular FAO is a crucial source of adenosine triphosphate (ATP) in podocytes, mitochondrial
335 respiration and ATP content were measured. Results showed that HG treatment decreased oxygen
336 consumption rate (OCR) and ATP content, whereas DAPA partially restored OCR and ATP levels
337 (Figure 3F). Additionally, DAPA significantly attenuated mitochondrial damage in podocytes (Figure
338 S1C). The expression of ERRα and ACOX1 was also assessed *in vitro*. Consistent with *in vivo* and
339 previous studies[39, 43, 44], HG-treated podocytes exhibited significant decreases in ERRα and
340 ACOX1 expression, as shown by immunofluorescence assays (Figure 3G) and Western blot analysis
341 (Figure 3H).

342 In contrast, DAPA pre-treatment upregulated ERRα and ACOX1 expression in podocytes,
343 partially reversing the decline caused by HG. These results suggest that decreased ERRα and ACOX1
344 expression induced by HG leads to compromised FA utilization and lipid accumulation in podocytes.
345 DAPA improves lipid metabolism by upregulating ERRα and ACOX1 expression in podocytes.

346

347 **Effects of the ERRα-ACOX1 axis on fatty acid utilization**

348 Previous studies confirmed ACOX1 as a potential target of ERRα by ChIP-on-chIP in mouse

349 kidney cells[45]. To determine whether ERRα is involved in fatty acid metabolism, podocytes were
350 transfected with an ERRα pcDNA recombinant or control plasmid and then incubated with HG.
351 Western blot analysis showed that ERRα overexpression significantly restored the diminished
352 expression of ACOX1 induced by HG, consistent with previous studies[39, 40] (Figure 4A-B). ERRα
353 overexpression also promoted lipid metabolism and utilization, evidenced by reduced lipid droplet
354 accumulation and decreased TG and FFA content under HG exposure (Figure 4C-G). Furthermore,
355 ERRα overexpression rescued the HG-induced decrease in OCR and ATP content in podocytes
356 (Figure 4H-I). In addition, immunofluorescence staining of TFAM (mitochondrial marker) showed
357 that overexpression of ERRα also attenuated HG-induced mitochondrial damage (Figure S2A). The
358 cell apoptosis rate was slightly reduced in podocytes transfected with ERRα plasmid under HG
359 conditions (Figure 4J). These results suggest ERRα regulates ACOX1 expression and participates in
360 podocyte fatty acid metabolism.

361

362 **Effects of specific knock-in of ERRα on ACOX1 expression in podocytes**

363 To further corroborate our hypothesis, podocyte-specific ERRα knock-in ($ERR\alpha^{podKI}$) mice were
364 generated using the Cre-LoxP system (Figure 5A). Conditional knock-in mice were identified by
365 sequencing genomic DNA (Figure 5B). Immunohistochemistry confirmed increased ERRα
366 expression in glomeruli from $ERR\alpha^{fl/fl}$/$NPHS2^{Cre+}$ mice ($ERR\alpha^{podKI}$) compared to $ERR\alpha^{fl/fl}$/
367 $NPHS2^{Cre-}$ mice ($ERR\alpha^{ctrl}$) (Figure 5C). Immunofluorescence co-staining (Figure 5D) and Real-time
368 PCR (Figure 5E) further validated these findings. Western blots showed that ACOX1 expression was
369 primarily increased in $ERR\alpha^{podKI}$ mice (Figure 5F), demonstrating *in vivo* a regulatory effect of ERRα
370 on ACOX1 expression, consistent with our *in vitro* studies.

371

372 **The protective effect of ERRα is reversed by the knockdown of ACOX1**

373 To further investigate the relationship between ERRα and ACOX1 *in vivo*, we constructed a DKD
374 model in ERRα$^{podKI/ctrl}$ mice using STZ. Subsequently, an adeno-associated virus (AAV) with
375 podocyte-specific ACOX1 knockdown was constructed and injected in situ into mouse kidneys
376 (Figure 6A). As anticipated from the *in vitro* experiments, overexpression of ERRα significantly
377 upregulated ACOX1 expression, as demonstrated by immunofluorescence and Western blot analyses
378 (Figure 6C-F). Additionally, the mRNA level of ACOX1 was significantly elevated (Figure 6G). In
379 the STZ-induced DKD model, ERRα^{podKI} mice exhibited markedly reduced levels of DKD injury
380 markers, including urea nitrogen, blood creatinine, and ACR, compared to controls (Figure 6B). The
381 overall degree of glomerular injury, evidenced by a significant reduction in the glomerulosclerosis
382 index and the fusion of podocyte foot processes, was also significantly improved (Figure 6H-I). In
383 addition, immunofluorescence staining of TFAM also showed that mitochondrial damage was
384 attenuated (Figure S3A). Furthermore, ERRα overexpression significantly attenuated glomerular
385 lipid accumulation (Figure 6J-K). However, the protective effect of ERRα was reversed after AAV-
386 mediated knockdown of ACOX1 expression (Figure 6B, 6H-K). These results suggest that ERRα
387 exerts its protective effects by upregulating ACOX1 expression.

388

389 **DAPA alleviated renal lipid accumulation and ameliorated kidney injury in STZ-induced**
390 **diabetic mice in an ERRα-dependent manner**

391 To clarify the therapeutic effect of DAPA on DKD, we used STZ to establish a high-fat diet
392 diabetic model in ERRα^{podKI} and ERRα^{ctrl} mice. The mice were treated with DAPA or vehicle control
393 (VEH) for 4 weeks (Figure 7A). Pathological markers of DKD, such as blood urea nitrogen (BUN),
394 serum creatinine (Cr), and ACR, were evaluated before sacrifice. DAPA treatment substantially

395 reduced the increased BUN, serum Cr, and ACR. ERRα knock-in mice showed a better therapeutic
396 response than those without the knock-in gene (Figure 7B). DAPA significantly reduced the overall
397 degree of glomerular injury in diabetic ERRα knock-in mice, as evidenced by a significantly lower
398 glomerulosclerosis index and improved fusion of podocyte foot processes compared to mice without
399 the knock-in gene (Figure 7C-D). In addition, immunofluorescence staining of TFAM also showed
400 that mitochondrial damage was attenuated (Figure S3B). We also measured glomerular lipid content
401 and found that ERRα knock-in enhanced the therapeutic effect of DAPA in reducing glomerular lipid
402 accumulation (Figure 7E-G). The expression of ERRα and ACOX1 was examined to elucidate the
403 molecular mechanism. Immunohistochemistry and immunofluorescence results, consistent with
404 Western blot and RT-PCR findings, showed that ERRα expression was upregulated by DAPA
405 treatment, and ACOX1 expression was further increased in ERRα knock-in mice (Figure 7H-K).
406 These data indicate that DAPA attenuates lipid accumulation primarily by enhancing ACOX1-
407 dependent lipid catabolism via an ERRα-dependent mechanism.
408

409 **Discussion**

410 Diabetic kidney disease (DKD) is one of the most prevalent and severe complications of diabetes,
411 affecting over 50% of individuals with diabetes and being associated with high morbidity and
412 mortality. Given the significant health risks and economic costs associated with DKD, there is a
413 pressing need to identify targeted agents that can effectively reverse its progression[46]. This study
414 has demonstrated that the expression of the transcription factor ERRα is significantly downregulated
415 in podocytes in the DKD state. This downregulation leads to marked inhibition of ACOX1-mediated
416 FAO, exacerbating lipotoxicity and promoting cellular damage. Additionally, we have found that the
417 SGLT2 inhibitor Dapagliflozin (DAPA) reverses ACOX1-mediated FAO by targeting and
418 upregulating ERRα expression, thereby attenuating lipotoxicity in DKD. These findings offer a novel
419 perspective on using SGLT2 inhibitors for treating DKD and reveal a distinctive therapeutic
420 mechanism by which these inhibitors enhance FAO in podocytes.

421 Currently, DKD treatment is primarily symptomatic, with no targeted agents available to reverse
422 its progression[47]. The main reason for the lack of effective therapeutic targets is the unclear
423 pathogenesis of DKD[48]. Major studies on DKD indicate that impaired glomerular structure and
424 function are crucial in its development[49]. Podocytes, the main components of the glomerulus, are
425 critically affected, with damage leading to significant renal function impairment[49]. In DKD,
426 podocytes undergo various injuries, including increased apoptosis and cell detachment, though the
427 specific mechanisms remain unclear[48]. Previous and recent studies have shown that FAO is
428 markedly suppressed in podocytes in the DKD state, resulting in lipotoxicity[4, 5, 50]. As a crucial
429 pathway for lipid degradation and energy supply, FAO is essential for podocyte lipid metabolism[7].
430 Moreover, as terminally differentiated cells, podocytes are particularly vulnerable to lipotoxicity,
431 underscoring the potential therapeutic value of targeting podocyte lipid metabolism[51].

432 Peroxisomal acyl-coenzyme A oxidases (ACOXs), the initial and rate-limiting enzymes of the
433 catalytic β-oxidation system in mitochondria, are highly expressed in organs such as the liver and
434 kidney[52]. ACOXs are classified into three isoforms: ACOX1, ACOX2, and ACOX3. Recent studies
435 have shown that ACOX1 plays a distinctive role in renal FAO and is significantly associated with
436 acute kidney injury and renal fibrosis[53, 54]. However, no studies have confirmed the role of
437 ACOX1 in podocytes. Our *in vivo* and *in vitro* experiments demonstrated for the first time that
438 ACOX1 expression was significantly downregulated in podocytes under DKD conditions, leading to
439 significant inhibition of its mediated lipid metabolism and exacerbated lipotoxicity, further promoting
440 podocyte injury. These findings suggest that ACOX1 and its mediated FAO represent important
441 therapeutic targets in DKD.

442 Despite numerous studies showing that ACOX1 expression is downregulated in various disease
443 models and associated with disease progression, the regulatory mechanism of ACOX1 has not been
444 confirmed[55-57]. The present study further explored the regulatory mechanism of ACOX1 in
445 podocytes. The results demonstrated that ACOX1 transcription was regulated by the transcription
446 factor ERRα, providing a new perspective on ACOX1 regulation in podocytes. ERRα is a crucial
447 nuclear transcription factor, metabolically active and highly expressed in organs, such as the liver,
448 skeletal muscle, and kidney[28]. Functionally, ERRα maintains membrane transport and energy
449 metabolism by regulating the transcription of downstream molecules[26]. ERRα is associated with
450 renal aging, acute kidney injury, and puromycin aminonucleoside-induced renal injury in renal
451 diseases, playing an important protective role[30, 32, 58]. Our previous study confirmed that
452 overexpression of ERRα by renal tubular epithelial cells significantly ameliorated renal tubular
453 pathological injury[39, 59], and in the present study we demonstrated that ERRα expression was
454 downregulated in podocytes and that overexpression of ERRα significantly ameliorated podocyte

455 injury in DKD. On the other hand, our previous study confirmed that in renal tubular cells, the level
456 of mRNA of ERRα was unchanged by HG stimulation, but its ubiquitination degradation was
457 increased, which in turn decreased its protein level[39]. However, there is still a lack of studies on the
458 changes in ERRα expression in podocytes and their specific mechanisms. In the present study, we
459 found that high glucose stimulation leads to a decrease in the protein level of ERRα, which is similar
460 to previous studies, but the specific mechanisms have not been further confirmed in the present study.
461 These differences may arise due to cell type–specific responses and the influence of post-translational
462 modifications.

463 Furthermore, our findings revealed that ERRα could regulate lipid metabolism by modulating
464 ACOX1 transcription. *In vivo* and *in vitro* experiments validated the binding sequences of ERRα and
465 ACOX1, elucidating the specific mechanisms through ERRα-mediated regulation. These results
466 confirm the importance of the ERRα-ACOX1 axis in FAO in DKD, suggesting that targeting this axis
467 in podocytes has therapeutic potential.

468 Large clinical cohort studies have confirmed the important role of SGLT2 inhibitors like DAPA
469 in DKD patients[60]. Recent studies have shown that DAPA significantly improves DKD patient
470 prognosis[10, 61]. However, the exact mechanisms remain unclear. SGLT2 is predominantly
471 expressed in proximal tubule cells, but recent studies have shown comparable SGLT2 expression in
472 podocytes [61]. DAPA's capacity to reduce podocyte lipotoxicity in experimental Alport syndrome
473 suggests a shared pathogenic mechanism with DKD. In both conditions, excess lipid accumulation in
474 podocytes leads to cellular dysfunction and detachment, contributing to glomerular injury. By
475 improving lipid metabolism and reducing lipotoxicity, DAPA may help preserve podocyte integrity,
476 thereby preventing the progression of DKD and improving overall renal function.[61].

Additionally, DAPA can reverse metabolic reprogramming by promoting FAO and inhibiting glycolysis, thus attenuating tubular cell injury. Interestingly, recent studies indicated that DAPA could act independently on SGLT2, extending its mechanisms of action[62, 63]. No studies have confirmed the therapeutic effects of DAPA on podocytes or elucidated its mechanisms. This study demonstrated for the first time that DAPA significantly improves FAO, and reduces lipotoxicity in high glucose-stimulated podocytes and glomeruli in a DKD animal model, exerting a vital renal protective effect. Furthermore, DAPA antagonized diabetes-induced decrease in ERRα and ACOX1 expression, and podocyte-specific overexpression of ERRα resulted in outcomes similar to DAPA treatment, suggesting that DAPA exerts its effects by upregulating ERRα expression in DKD. These findings provide new insights into the action mechanisms of action of DAPA.

While our study yielded promising results, several limitations should be considered. First, extending the intervention period could provide insights into the long-term therapeutic effects and disease progression. Second, the role of ACOX1 overexpression in vivo was not further explored. Finally, analyzing kidney specimens from DKD patients may further confirm our animal experiment findings.

In conclusion, our study supports the hypothesis that the downregulation of ERRα expression in podocytes under DKD conditions inhibits ACOX1-mediated FAO, promoting lipotoxicity and subsequent podocyte injury. DAPA administration significantly ameliorates lipotoxicity and attenuates podocyte injury by upregulating the ERRα-ACOX1 axis. This provides a novel perspective on the mechanism of action of SGLT2 inhibitors in DKD.

Acknowledgements

We are grateful for the technical support for immunofluorescence provided by Hubei BIOSSCI Biotech Co., Ltd (Wuhan Changyan Pathology technology Co., Ltd).

Authors' contributions

Hongtu Hu: Writing– review & editing, Supervision, Project administration, Conceptualization. Juan Wang: review & editing, Supervision, Project administration, Funding acquisition. Zhuan Peng: Validation, Methodology. Keju Yang: Validation, Methodology. Weiwei Li: Validation, Methodology. Yanqin Fan: Validation, Methodology. Qian Yang: Validation, Methodology, Funding acquisition. Jijia Hu: Writing– review & editing, Supervision, Project administration, Funding acquisition, Conceptualization.

Funding

This study was supported by the National Natural Science Foundation of China (82300767 to J. Hu, 82270710 to Q. Yang and 82100705 to Y. Fan).

Data Availability Statement

The data that support the findings of this study are available from the corresponding author upon reasonable request.

Declarations

Ethics approval and consent to participate

This study was approved by the Ethics Committee of Renmin Hospital of Wuhan University, and participants who provided informed consent (WDRY2021-KS034) were granted access to digital medical records.

Consent for publication

Not applicable.

Competing interests

No potential conflicts of interest relevant to this article were reported.

530 # References

531 [1] S. Gupta, M. Dominguez, L. Golestaneh, Diabetic Kidney Disease: An Update, Med Clin North
532 Am 107(4) (2023) 689-705.

533 [2] L. Opazo-Rios, S. Mas, G. Marin-Royo, S. Mezzano, C. Gomez-Guerrero, J.A. Moreno, J. Egido,
534 Lipotoxicity and Diabetic Nephropathy: Novel Mechanistic Insights and Therapeutic Opportunities,
535 Int J Mol Sci 21(7) (2020).

536 [3] M. Fontecha-Barriuso, D. Martin-Sanchez, J.M. Martinez-Moreno, M. Monsalve, A.M. Ramos,
537 M.D. Sanchez-Nino, M. Ruiz-Ortega, A. Ortiz, A.B. Sanz, The Role of PGC-1alpha and
538 Mitochondrial Biogenesis in Kidney Diseases, Biomolecules 10(2) (2020).

539 [4] Z. Luo, Z. Chen, J. Hu, G. Ding, Interplay of lipid metabolism and inflammation in podocyte
540 injury, Metabolism 150 (2024) 155718.

541 [5] Y. Hao, Y. Fan, J. Feng, Z. Zhu, Z. Luo, H. Hu, W. Li, H. Yang, G. Ding, ALCAT1-mediated
542 abnormal cardiolipin remodelling promotes mitochondrial injury in podocytes in diabetic kidney
543 disease, Cell Commun Signal 22(1) (2024) 26.

544 [6] F. Zuo, Y. Wang, X. Xu, R. Ding, W. Tang, Y. Sun, X. Wang, Y. Zhang, J. Wu, Y. Xie, M. Liu, Z.
545 Wang, F. Yi, CCDC92 deficiency ameliorates podocyte lipotoxicity in diabetic kidney disease,
546 Metabolism 150 (2024) 155724.

547 [7] Z. Gai, T. Wang, M. Visentin, G.A. Kullak-Ublick, X. Fu, Z. Wang, Lipid Accumulation and
548 Chronic Kidney Disease, Nutrients 11(4) (2019).

549 [8] X.X. Wang, M.H. Edelstein, U. Gafter, L. Qiu, Y. Luo, E. Dobrinskikh, S. Lucia, L. Adorini, V.D.
550 D'Agati, J. Levi, A. Rosenberg, J.B. Kopp, D.R. Gius, M.A. Saleem, M. Levi, G Protein-Coupled
551 Bile Acid Receptor TGR5 Activation Inhibits Kidney Disease in Obesity and Diabetes, J Am Soc
552 Nephrol 27(5) (2016) 1362-78.

553 [9] K.R. Tuttle, R. Agarwal, C.E. Alpers, G.L. Bakris, F.C. Brosius, P. Kolkhof, J. Uribarri, Molecular
554 mechanisms and therapeutic targets for diabetic kidney disease, Kidney Int 102(2) (2022) 248-260.
555 [10] S. Dhillon, Dapagliflozin: A Review in Type 2 Diabetes, Drugs 79(10) (2019) 1135-1146.
556 [11] D.C. Wheeler, B.V. Stefansson, N. Jongs, G.M. Chertow, T. Greene, F.F. Hou, J.J.V. McMurray,
557 R. Correa-Rotter, P. Rossing, R.D. Toto, C.D. Sjostrom, A.M. Langkilde, H.J.L. Heerspink, D.-C.T.
558 Committees, Investigators, Effects of dapagliflozin on major adverse kidney and cardiovascular
559 events in patients with diabetic and non-diabetic chronic kidney disease: a prespecified analysis from
560 the DAPA-CKD trial, Lancet Diabetes Endocrinol 9(1) (2021) 22-31.
561 [12] H.J.L. Heerspink, B.V. Stefansson, R. Correa-Rotter, G.M. Chertow, T. Greene, F.F. Hou, J.F.E.
562 Mann, J.J.V. McMurray, M. Lindberg, P. Rossing, C.D. Sjostrom, R.D. Toto, A.M. Langkilde, D.C.
563 Wheeler, D.-C.T. Committees, Investigators, Dapagliflozin in Patients with Chronic Kidney Disease,
564 N Engl J Med 383(15) (2020) 1436-1446.
565 [13] S.I. Taylor, Z.S. Yazdi, A.L. Beitelshees, Pharmacological treatment of hyperglycemia in type 2
566 diabetes, J Clin Invest 131(2) (2021).
567 [14] J. Wei, F. Tan, X. Long, Q. Fang, Y. Wang, J. Wang, J. He, X. Yuan, J. Du, RNA-Seq
568 transcriptome analysis of renal tissue from spontaneously hypertensive rats revealed renal protective
569 effects of dapagliflozin, an inhibitor of sodium-glucose cotransporter 2, Eur J Pharm Sci 189 (2023)
570 106531.
571 [15] J. Sun, X. Zhang, S. Wang, D. Chen, J. Shu, N. Chong, Q. Wang, Y. Xu, Dapagliflozin improves
572 podocytes injury in diabetic nephropathy via regulating cholesterol balance through KLF5 targeting
573 the ABCA1 signalling pathway, Diabetol Metab Syndr 16(1) (2024) 38.
574 [16] B. Feng, F. Yang, J. Liu, Q. Sun, R. Meng, D. Zhu, Amelioration of diabetic kidney injury with
575 dapagliflozin is associated with suppressing renal HMGB1 expression and restoring autophagy in

576 obese mice, J Diabetes Complications 37(3) (2023) 108409.

577 [17] A. He, X. Chen, M. Tan, Y. Chen, D. Lu, X. Zhang, J.M. Dean, B. Razani, I.J. Lodhi, Acetyl-
578 CoA Derived from Hepatic Peroxisomal beta-Oxidation Inhibits Autophagy and Promotes Steatosis
579 via mTORC1 Activation, Mol Cell 79(1) (2020) 30-42 e4.

580 [18] J. Kalucka, L. Bierhansl, N.V. Conchinha, R. Missiaen, I. Elia, U. Bruning, S. Scheinok, L. Treps,
581 A.R. Cantelmo, C. Dubois, P. de Zeeuw, J. Goveia, A. Zecchin, F. Taverna, F. Morales-Rodriguez, A.
582 Brajic, L.C. Conradi, S. Schoors, U. Harjes, K. Vriens, G.A. Pilz, R. Chen, R. Cubbon, B. Thienpont,
583 B. Cruys, B.W. Wong, B. Ghesquiere, M. Dewerchin, K. De Bock, X. Sagaert, S. Jessberger, E.A.V.
584 Jones, B. Gallez, D. Lambrechts, M. Mazzone, G. Eelen, X. Li, S.M. Fendt, P. Carmeliet, Quiescent
585 Endothelial Cells Upregulate Fatty Acid beta-Oxidation for Vasculoprotection via Redox
586 Homeostasis, Cell Metab 28(6) (2018) 881-894 e13.

587 [19] F. Huang, S. Wang, A. Zhao, X. Zheng, Y. Zhang, S. Lei, K. Ge, C. Qu, Q. Zhao, C. Yan, W. Jia,
588 Pu-erh Tea Regulates Fatty Acid Metabolism in Mice Under High-Fat Diet, Front Pharmacol 10 (2019)
589 63.

590 [20] K.S. Collins, M.T. Eadon, Y.H. Cheng, D. Barwinska, R. Melo Ferreira, T.W. McCarthy, D.
591 Janosevic, F. Syed, B. Maier, T.M. El-Achkar, K.J. Kelly, C.L. Phillips, T. Hato, T.A. Sutton, P.C.
592 Dagher, Alterations in Protein Translation and Carboxylic Acid Catabolic Processes in Diabetic
593 Kidney Disease, Cells 11(7) (2022).

594 [21] Q. Rong, B. Han, Y. Li, H. Yin, J. Li, Y. Hou, Berberine Reduces Lipid Accumulation by
595 Promoting Fatty Acid Oxidation in Renal Tubular Epithelial Cells of the Diabetic Kidney, Front
596 Pharmacol 12 (2021) 729384.

597 [22] N. Chen, L. Mu, Z. Yang, C. Du, M. Wu, S. Song, C. Yuan, Y. Shi, Carbohydrate response
598 element-binding protein regulates lipid metabolism via mTOR complex1 in diabetic nephropathy, J

599 Cell Physiol 236(1) (2021) 625-640.

600 [23] H. Yaribeygi, M. Maleki, Z. Reiner, T. Jamialahmadi, A. Sahebkar, Mechanistic View on the
601 Effects of SGLT2 Inhibitors on Lipid Metabolism in Diabetic Milieu, J Clin Med 11(21) (2022).

602 [24] L. Li, Q. Li, W. Huang, Y. Han, H. Tan, M. An, Q. Xiang, R. Zhou, L. Yang, Y. Cheng,
603 Dapagliflozin Alleviates Hepatic Steatosis by Restoring Autophagy via the AMPK-mTOR Pathway,
604 Front Pharmacol 12 (2021) 589273.

605 [25] C. Billon, E. Schoepke, A. Avdagic, A. Chatterjee, A.A. Butler, B. Elgendy, J.K. Walker, T.P.
606 Burris, A Synthetic ERR Agonist Alleviates Metabolic Syndrome, J Pharmacol Exp Ther 388(2)
607 (2024) 232-240.

608 [26] M. Tripathi, P.M. Yen, B.K. Singh, Estrogen-Related Receptor Alpha: An Under-Appreciated
609 Potential Target for the Treatment of Metabolic Diseases, Int J Mol Sci 21(5) (2020).

610 [27] C. Cerutti, J.R. Shi, J.M. Vanacker, Multifaceted Transcriptional Network of Estrogen-Related
611 Receptor Alpha in Health and Disease, Int J Mol Sci 24(5) (2023).

612 [28] P. Dhillon, J. Park, C. Hurtado Del Pozo, L. Li, T. Doke, S. Huang, J. Zhao, H.M. Kang, R.
613 Shrestra, M.S. Balzer, S. Chatterjee, P. Prado, S.Y. Han, H. Liu, X. Sheng, P. Dierickx, K. Batmanov,
614 J.P. Romero, F. Prosper, M. Li, L. Pei, J. Kim, N. Montserrat, K. Susztak, The Nuclear Receptor
615 ESRRA Protects from Kidney Disease by Coupling Metabolism and Differentiation, Cell Metab 33(2)
616 (2021) 379-394 e8.

617 [29] S. Spinelli, M. Bruschi, M. Passalacqua, L. Guida, M. Magnone, L. Sturla, E. Zocchi, Estrogen-
618 Related Receptor alpha: A Key Transcription Factor in the Regulation of Energy Metabolism at an
619 Organismic Level and a Target of the ABA/LANCL Hormone Receptor System, Int J Mol Sci 25(9)
620 (2024).

621 [30] X.X. Wang, K. Myakala, A.E. Libby, E. Krawczyk, J. Panov, B.A. Jones, K. Bhasin, N. Shults,

622 Y. Qi, K.W. Krausz, P.M. Zerfas, S. Takahashi, P. Daneshpajouhnejad, A. Titievsky, E. Taranenko, C.
623 Billon, A. Chatterjee, B. Elgendy, J.K. Walker, C. Albanese, J.B. Kopp, A.Z. Rosenberg, F.J. Gonzalez,
624 U. Guha, L. Brodsky, T.P. Burris, M. Levi, Estrogen-Related Receptor Agonism Reverses
625 Mitochondrial Dysfunction and Inflammation in the Aging Kidney, Am J Pathol 193(12) (2023) 1969-
626 1987.
627 [31] K. Kitamura, J.S. Erlangga, S. Tsukamoto, Y. Sakamoto, H. Mabashi-Asazuma, K. Iida, Daidzein
628 promotes the expression of oxidative phosphorylation- and fatty acid oxidation-related genes via an
629 estrogen-related receptor alpha pathway to decrease lipid accumulation in muscle cells, J Nutr
630 Biochem 77 (2020) 108315.
631 [32] K. Tsushida, K. Tanabe, K. Masuda, S. Tanimura, H. Miyake, Y. Arata, H. Sugiyama, J. Wada,
632 Estrogen-related receptor alpha is essential for maintaining mitochondrial integrity in cisplatin-
633 induced acute kidney injury, Biochem Biophys Res Commun 498(4) (2018) 918-924.
634 [33] X. Yang, Z. Chen, Z. Luo, D. Yang, Y. Hao, J. Hu, J. Feng, Z. Zhu, Q. Luo, Z. Zhang, W. Liang,
635 G. Ding, STING deletion alleviates podocyte injury through suppressing inflammation by targeting
636 NLRP3 in diabetic kidney disease, Cell Signal 109 (2023) 110777.
637 [34] Q. Yang, J. Hu, Y. Yang, Z. Chen, J. Feng, Z. Zhu, H. Wang, D. Yang, W. Liang, G. Ding, Sirt6
638 deficiency aggravates angiotensin II-induced cholesterol accumulation and injury in podocytes,
639 Theranostics 10(16) (2020) 7465-7479.
640 [35] Z. Chen, Z. Zhu, W. Liang, Z. Luo, J. Hu, J. Feng, Z. Zhang, Q. Luo, H. Yang, G. Ding, Reduction
641 of anaerobic glycolysis contributes to angiotensin II-induced podocyte injury with foot process
642 effacement, Kidney Int 103(4) (2023) 735-748.
643 [36] M.A. Saleem, M.J. O'Hare, J. Reiser, R.J. Coward, C.D. Inward, T. Farren, C.Y. Xing, L. Ni,
644 P.W. Mathieson, P. Mundel, A conditionally immortalized human podocyte cell line demonstrating

645 nephrin and podocin expression, J Am Soc Nephrol 13(3) (2002) 630-638.

646 [37] Y.H. Wang, D.Y. Chang, M.H. Zhao, M. Chen, Dapagliflozin Alleviates Diabetic Kidney Disease
647 via Hypoxia Inducible Factor 1alpha/Heme Oxygenase 1-Mediated Ferroptosis, Antioxid Redox
648 Signal 40(7-9) (2024) 492-509.

649 [38] A. Cai, J. Shen, X. Yang, X. Shao, L. Gu, S. Mou, X. Che, Dapagliflozin alleviates renal
650 inflammation and protects against diabetic kidney diseases, both dependent and independent of blood
651 glucose levels, Front Immunol 14 (2023) 1205834.

652 [39] H. Hu, J. Hu, Z. Chen, K. Yang, Z. Zhu, Y. Hao, Z. Zhang, W. Li, Z. Peng, Y. Cao, X. Sun, F.
653 Zhang, Q. Chi, G. Ding, W. Liang, RBBP6-Mediated ERRα Degradation Contributes to
654 Mitochondrial Injury in Renal Tubular Cells in Diabetic Kidney Disease, Adv Sci (Weinh) 11(46)
655 (2024) e2405153.

656 [40] K. Yang, W. Liang, H. Hu, Z. Zhang, Y. Hao, Z. Song, L. Yang, J. Hu, Z. Chen, G. Ding, ESRRA
657 modulation by empagliflozin mitigates diabetic tubular injury via mitochondrial restoration, Cell
658 Signal 122 (2024) 111308.

659 [41] O.P. Nordbo, L. Landolt, O. Eikrem, A. Scherer, S. Leh, J. Furriol, T. Apeland, P. Mydel, H.P.
660 Marti, Transcriptomic analysis reveals partial epithelial-mesenchymal transition and inflammation as
661 common pathogenic mechanisms in hypertensive nephrosclerosis and Type 2 diabetic nephropathy,
662 Physiol Rep 11(19) (2023) e15825.

663 [42] J.A. Schaub, F.M. AlAkwaa, P.J. McCown, A.S. Naik, V. Nair, S. Eddy, R. Menon, E.A. Otto, D.
664 Demeke, J. Hartman, D. Fermin, C.L. O'Connor, L. Subramanian, M. Bitzer, R. Harned, P. Ladd, L.
665 Pyle, S. Pennathur, K. Inoki, J.B. Hodgin, F.C. Brosius, 3rd, R.G. Nelson, M. Kretzler, P. Bjornstad,
666 SGLT2 inhibitors mitigate kidney tubular metabolic and mTORC1 perturbations in youth-onset type
667 2 diabetes, J Clin Invest 133(5) (2023).

[43] D. Wang, Y. Wang, F.Q. Liu, Z.Y. Yuan, J.J. Mu, High Salt Diet Affects Renal Sodium Excretion and ERRalpha Expression, Int J Mol Sci 17(4) (2016) 480.

[44] W. Xia, Z. Pan, H. Zhang, Q. Zhou, Y. Liu, ERRalpha protects against sepsis-induced acute lung injury in rats, Mol Med 29(1) (2023) 76.

[45] A.M. Tremblay, C.R. Dufour, M. Ghahremani, T.L. Reudelhuber, V. Giguere, Physiological genomics identifies estrogen-related receptor alpha as a regulator of renal sodium and potassium homeostasis and the renin-angiotensin pathway, Mol Endocrinol 24(1) (2010) 22-32.

[46] H.J. Anders, T.B. Huber, B. Isermann, M. Schiffer, CKD in diabetes: diabetic kidney disease versus nondiabetic kidney disease, Nat Rev Nephrol 14(6) (2018) 361-377.

[47] M. Akhtar, N.M. Taha, A. Nauman, I.B. Mujeeb, A. Al-Nabet, Diabetic Kidney Disease: Past and Present, Adv Anat Pathol 27(2) (2020) 87-97.

[48] S. Rayego-Mateos, R.R. Rodrigues-Diez, B. Fernandez-Fernandez, C. Mora-Fernandez, V. Marchant, J. Donate-Correa, J.F. Navarro-Gonzalez, A. Ortiz, M. Ruiz-Ortega, Targeting inflammation to treat diabetic kidney disease: the road to 2030, Kidney Int 103(2) (2023) 282-296.

[49] J. Fu, K.M. Akat, Z. Sun, W. Zhang, D. Schlondorff, Z. Liu, T. Tuschl, K. Lee, J.C. He, Single-Cell RNA Profiling of Glomerular Cells Shows Dynamic Changes in Experimental Diabetic Kidney Disease, J Am Soc Nephrol 30(4) (2019) 533-545.

[50] H. Qu, X. Liu, J. Zhu, X. Xiong, L. Li, Q. He, Y. Wang, G. Yang, L. Zhang, Q. Yang, G. Luo, Y. Zheng, H. Zheng, Dock5 Deficiency Promotes Proteinuric Kidney Diseases via Modulating Podocyte Lipid Metabolism, Adv Sci (Weinh) 11(11) (2024) e2306365.

[51] C. Mayrhofer, S. Krieger, N. Huttary, M.W. Chang, J. Grillari, G. Allmaier, D. Kerjaschki, Alterations in fatty acid utilization and an impaired antioxidant defense mechanism are early events in podocyte injury: a proteomic analysis, Am J Pathol 174(4) (2009) 1191-202.

691 [52] S.M. Houten, S. Violante, F.V. Ventura, R.J. Wanders, The Biochemistry and Physiology of
692 Mitochondrial Fatty Acid beta-Oxidation and Its Genetic Disorders, Annu Rev Physiol 78 (2016) 23-
693 44.
694 [53] J. Chen, Q.Y. Zheng, L.M. Wang, J. Luo, K.H. Chen, Y.N. He, Proteomics reveals defective
695 peroxisomal fatty acid oxidation during the progression of acute kidney injury and repair, Heliyon
696 9(7) (2023) e18134.
697 [54] Y.H. Zhang, L. Bin, Q. Meng, D. Zhang, H. Yang, G. Li, Y. Wang, M. Liu, N. Liu, J. Yu, S. Liu,
698 H. Zhou, Z.X. Xu, Y. Wang, ACOX1 deficiency-induced lipid metabolic disorder facilitates chronic
699 interstitial fibrosis development in renal allografts, Pharmacol Res 201 (2024) 107105.
700 [55] H.S. Park, J.W. Song, J.H. Park, B.K. Lim, O.S. Moon, H.Y. Son, J.H. Lee, B. Gao, Y.S. Won,
701 H.J. Kwon, TXNIP/VDUP1 attenuates steatohepatitis via autophagy and fatty acid oxidation,
702 Autophagy 17(9) (2021) 2549-2564.
703 [56] H.L. Chung, M.F. Wangler, P.C. Marcogliese, J. Jo, T.A. Ravenscroft, Z. Zuo, L. Duraine, S.
704 Sadeghzadeh, D. Li-Kroeger, R.E. Schmidt, A. Pestronk, J.A. Rosenfeld, L. Burrage, M.J. Herndon,
705 S. Chen, N. Members of Undiagnosed Diseases, A. Shillington, M. Vawter-Lee, R. Hopkin, J.
706 Rodriguez-Smith, M. Henrickson, B. Lee, A.B. Moser, R.O. Jones, P. Watkins, T. Yoo, S. Mar, M.
707 Choi, R.C. Bucelli, S. Yamamoto, H.K. Lee, C.E. Prada, J.H. Chae, T.P. Vogel, H.J. Bellen, Loss- or
708 Gain-of-Function Mutations in ACOX1 Cause Axonal Loss via Different Mechanisms, Neuron 106(4)
709 (2020) 589-606 e6.
710 [57] Q. Zhang, X. Yang, J. Wu, S. Ye, J. Gong, W.M. Cheng, Z. Luo, J. Yu, Y. Liu, W. Zeng, C. Liu,
711 Z. Xiong, Y. Chen, Z. He, P. Lan, Reprogramming of palmitic acid induced by dephosphorylation of
712 ACOX1 promotes beta-catenin palmitoylation to drive colorectal cancer progression, Cell Discov 9(1)
713 (2023) 26.

714 [58] Y. Muroya, O. Ito, R. Rong, K. Takashima, D. Ito, P. Cao, Y. Nakamura, K. Joh, M. Kohzuki,
715 Disorder of fatty acid metabolism in the kidney of PAN-induced nephrotic rats, Am J Physiol Renal
716 Physiol 303(7) (2012) F1070-9.
717 [59] H. Hu, W. Li, Y. Hao, Z. Peng, Z. Zou, J. Wei, Y. Zhou, W. Liang, Y. Cao, The SGLT2 inhibitor
718 dapagliflozin ameliorates renal fibrosis in hyperuricemic nephropathy, Cell Rep Med 5(8) (2024)
719 101690.
720 [60] P. McEwan, P.D. Gabb, J.A. Davis, J.J.G. Sanchez, C.D. Sjostrom, S. Barone, P. Kashioulis, M.
721 Ouwens, S. Cassimaty, R. Correa-Rotter, P. Rossing, D.C. Wheeler, H.J.L. Heerspink, The long-term
722 effects of dapagliflozin in chronic kidney disease: a time-to-event analysis, Nephrol Dial Transplant
723 (2024).
724 [61] M. Ge, J. Molina, J.J. Kim, S.K. Mallela, A. Ahmad, J. Varona Santos, H. Al-Ali, A. Mitrofanova,
725 K. Sharma, F. Fontanesi, S. Merscher, A. Fornoni, Empagliflozin reduces podocyte lipotoxicity in
726 experimental Alport syndrome, Elife 12 (2023).
727 [62] Q. Wu, Q. Yao, T. Hu, J. Yu, K. Jiang, Y. Wan, Q. Tang, Dapagliflozin protects against chronic
728 heart failure in mice by inhibiting macrophage-mediated inflammation, independent of SGLT2, Cell
729 Rep Med 4(12) (2023) 101334.
730 [63] A. Kogot-Levin, Y. Riahi, I. Abramovich, O. Mosenzon, B. Agranovich, L. Kadosh, R. Ben-
731 Haroush Schyr, D. Kleiman, L. Hinden, E. Cerasi, D. Ben-Zvi, E. Bernal-Mizrachi, J. Tam, E.
732 Gottlieb, G. Leibowitz, Mapping the metabolic reprogramming induced by sodium-glucose
733 cotransporter 2 inhibition, JCI Insight 8(7) (2023).
734

735 ## Figure legends

736 **Figure 1. Effect of DAPA on diabetes-induced glomerular lipid accumulation**

737 **(A)** Schematic diagram of 4-week treatment of 1 mg/kg dagliflozin (DAPA) or normal saline (Vehicle)
738 to db/db mice.

739 **(B)** Serum ACR levels in each mouse group.

740 **(C-D)** Representative images of PAS stainings and quantification of mesangial matrix expansion of
741 glomeruli from each group of mice.

742 **(E)** Representative images of TEM and quantification of foot process width from each group of mice.

743 **(F-G)** Triglyceride (TG) and free fatty acid (FFA) contents in glomeruli of mice in each group.

744 **(H-I)** Representative images and quantification of Oil Red O (ORO) stanings of glomeruli from each
745 group of mice.

746 **(J-K)** Representative images and quantification of BODIPY stanings of glomeruli from each group
747 of mice.

748 n=6 independent group mice. Data are expressed as mean ± SD. Statistical differences among three
749 or more groups were evaluated using one-way ANOVA followed by Tukey's post hoc test. *** $P <$
750 0.001.

751

752 **Figure 2. Effects of DAPA on the expression of ERRα and ACOX1**

753 **(A)** Chord plots showing KEGG-enriched items of DEGs in kidneys from patients (GSE166239) of
754 the control group versus the DKD group.

755 **(B)** Heatmap showing the alterations of fatty acid oxidation (FAO) related gene expression in kidneys
756 from patients (GSE166239) of the control group versus the DKD group.

757 **(C)** Correlation analysis of glomerular filtration rate (GFR) and ACOX1 expression in DKD patients
758 (using nephroseq).

759 **(D)** Correlation analysis of GFR and ERRα expression in DKD patients (using nephroseq).

760 **(E)** ScRNA-seq (GSE220939) depicted podocytes (POD), ACOX1-positive cell localization, and
761 ACOX1's expression in the POD cluster from each patient group.

762 **(F-G)** Representative images and quantification of immunohistochemical stainings in glomeruli of
763 mice and patients from each group.

764 **(H)** Representative images and quantification of ACOX1 (red), ERRα (green), WT1 (grey), and DAPI
765 (blue)-immunofluorescent stained kidney sections in glomeruli of mice from each group.

766 **(I)** Representative images and band density quantification of Western blots using isolated glomeruli
767 from each mouse group to quantify protein expression of ACOX1 and ERRα normalized to β-actin.
768 n=6 independent group mice. Control, control patients; DKD, diabetic kidney disease patients. Data
769 are expressed as mean ± SD. Statistical differences among three or more groups were evaluated using
770 one-way ANOVA followed by Tukey's post hoc test. * $P < 0.05$; ** $P < 0.01$; *** $P < 0.001$.
771

772 **Figure 3. DAPA treatment mitigated high glucose-induced lipids accumulation in vitro**
773 **(A)** Representative images and quantification of Oil Red O (ORO) stanings of podocytes from each
774 group.
775 **(B)** Representative images and quantification of BODIPY stanings of podocytes from each group.
776 **(C-D)** Triglyceride (TG) and free fatty acid (FFA) contents of podocytes from each group.
777 **(E)** Flow cytometry analysis of the apoptotic rate of podocytes from each group.
778 **(F)** OCR and ATP contents measurement experiment performed on podocytes from each group.
779 **(G)** Representative images and quantification of ACOX1 (red), ERRα (green) and DAPI (blue)-
780 immunofluorescent stained podocytes from each group.
781 **(H)** Representative images and band density quantification of Western blots using podocytes from
782 each group to quantify protein expression of ACOX1 and ERRα normalized to β-actin.
783 n=3 cultures per group. HG, high gluose (30mM, 24h); DAPA, dapagliflozin (10 μM, 24h). Data are
784 expressed as mean ± SD. Statistical differences among three or more groups were evaluated using
785 one-way ANOVA followed by Tukey's post hoc test. * $P < 0.05$, ** $P < 0.01$, *** $P < 0.001$.
786

787 **Figure 4. Effects of the ERRα-ACOX1 axis on fatty acids utilization.**
788 **(A)** Representative images and band density quantification of Western blots using podocytes from
789 each group to quantify protein expression of ACOX1 and ERRα normalized to β-actin.
790 **(B)** Representative images and quantification of ACOX1 (red), ERRα (green) and DAPI (blue)-
791 immunofluorescent stained podocytes from each group.
792 **(C)** Representative images and quantification of Oil Red O (ORO) stanings of podocytes from each
793 group.
794 **(D-E)** Representative images and quantification of BODIPY stanings of podocytes from each group.
795 **(F-G)** Triglyceride (TG) and free fatty acid (FFA) contents of podocytes from each group.
796 **(H-I)** OCR and ATP contents measurement experiment performed on podocytes from each group.

797 **(J)** Flow cytometry analysis of the apoptotic rate of podocytes from each group.
798 n=3 cultures per group. HG, High gluose (30mM, 24h); OE-ERRα, overexpression ERRα group. Data
799 are expressed as mean ± SD. Statistical differences among three or more groups were evaluated using
800 one-way ANOVA followed by Tukey's post hoc test. ns: not significant ($P > 0.05$), ** $P < 0.01$, ***
801 $P < 0.001$.
802
803 **Figure 5. Effects of specific knock-in of ERRα on ACOX1 expression in podocytes.**
804 **(A)** Schematic diagram of $ERR\alpha^{podKI}$ mice.
805 **(B)** Genotyping the mice by PCR analysis of genomic DNA, lanes 1-4 are $ERR\alpha^{ctrl}$ genotype, lane 3
806 is $ERR\alpha^{podKI}$ genotype.
807 **(C)** Representative images and quantification of immunohistochemical stainings in glomeruli of mice
808 from each group.
809 **(D)** Representative images and quantification of ACOX1 (red), ERRα (green), WT1 (grey), and DAPI
810 (blue)-immunofluorescent stained kidney sections in glomeruli of mice from each group.
811 **(E)** Relative mRNA levels of ACOX1 and ERRα in glomeruli of mice from each group.
812 **(F)** Representative images and band density quantification of Western blots using isolated glomeruli
813 from each mouse group to quantify protein expression of ACOX1 and ERRα normalized to β-actin.
814 n=6 independent group mice. $ERR\alpha^{ctrl}$, control mice; $ERR\alpha^{podKI}$, podocyte-specific knock-in mice.
815 Data are expressed as mean ± SD. Statistical differences among three or more groups were evaluated
816 using one-way ANOVA followed by Tukey's post hoc test. *** $P < 0.001$.
817
818 **Figure 6. The protective effect of ERRα is reversed by the knockdown of ACOX1.**
819 **(A)** Schematic diagram of intraperitoneal injection of Streptozotocin (STZ) and adeno-associated
820 virus (AAV) injection to $ERR\alpha^{podKI}$ mice.
821 **(B)** Serum BUN, Cr, and ACR levels in each mouse group.
822 **(C-D)** Representative images and quantification of ACOX1 (red), ERRα (green), WT1 (grey), and
823 DAPI (blue)-immunofluorescent stained kidney sections in glomeruli of mice from each group.
824 **(E-F)** Representative images and band density quantification of Western blots using isolated
825 glomeruli from each mouse group to quantify protein expression of ACOX1 and ERRα normalized
826 to β-actin.
827 **(G)** Relative mRNA levels of ACOX1 and ERRα in glomeruli of mice from each group.

828 Data are presented as means ± SD. ns: not significant ($P > 0.05$), ** $P < 0.01$, *** $P < 0.001$.
829 **(H)** Representative imagesf PAS stanings and quantification of mesangial matrix expansion from
830 each group of mice.
831 **(I)** Representative images of TEM and quantification of foot process width from each group of mice.
832 **(J)** Representative images and quantification of BODIPY stanings of glomeruli from each group of
833 mice.
834 **(K)** Representative images and quantification of Oil Red O stanings of glomeruli from each group of
835 mice.
836 n=6 independent group mice. ERRα^{ctrl}, control mice; ERRα^{podKI}, podocyte-specific knock-in mice;
837 shNC, empty AAV injection group; shACOX1, knockdown of ACOX1 expression group using AAV.
838 Data are expressed as mean ± SD. Statistical differences among three or more groups were evaluated
839 using one-way ANOVA followed by Tukey's post hoc test. ns: not significant ($P > 0.05$), * $P < 0.05$,
840 ** $P < 0.01$, *** $P < 0.001$.
841
842 **Figure7. DAPA alleviated renal lipid accumulation and ameliorated kidney injury in STZ-**
843 **induced diabetic mice in an ERRα-dependent manner.**
844 **(A)** Schematic diagram of intraperitoneal injection of Streptozotocin (STZ) and 4-week treatment of
845 1 mg/kg dagliflozin (DAPA) or normal saline (Vehicle) to ERRα^{podKI} mice.
846 **(B)** Serum BUN, Cr, and ACR levels in each mouse group.
847 **(C)** Representative imagesf PAS stanings and quantification of mesangial matrix expansion from each
848 group of mice.
849 **(D)** Representative images of TEM and quantification of foot process width from each group of mice.
850 **(E)** Representative images and quantification of Oil Red O (ORO) and BODIPY stanings of glomeruli
851 from each group of mice.
852 **(F-G)** Triglyceride (TG) and free fatty acid (FFA) contents in glomeruli of mice in each group.
853 **(H)** Representative images and quantification of immunohistochemical stainings in glomeruli of mice
854 from each group.
855 **(I)** Representative images and quantification of ACOX1 (red), ERRα (green), WT1 (grey), and DAPI
856 (blue)-immunofluorescent stained kidney sections in glomeruli of mice from each group.
857 **(J)** Representative images and band density quantification of Western blots using isolated glomeruli
858 from each mouse group to quantify protein expression of ACOX1 and ERRα normalized to β-actin.

859 **(K)** Relative mRNA levels of ACOX1 and ERRα in glomeruli of mice from each group.
860 n=6 independent group mice. VEH, saline; DAPA, dapagliflozin; ERRα^{ctrl}, control mice; ERRα^{podKI},
861 podocyte-specific knock-in mice. Data are expressed as mean ± SD. Statistical differences among
862 three or more groups were evaluated using one-way ANOVA followed by Tukey's post hoc test. ns:
863 not significant ($P > 0.05$), * $P < 0.05$, ** $P < 0.01$, *** $P < 0.001$.
864

865 **Figure 1.**

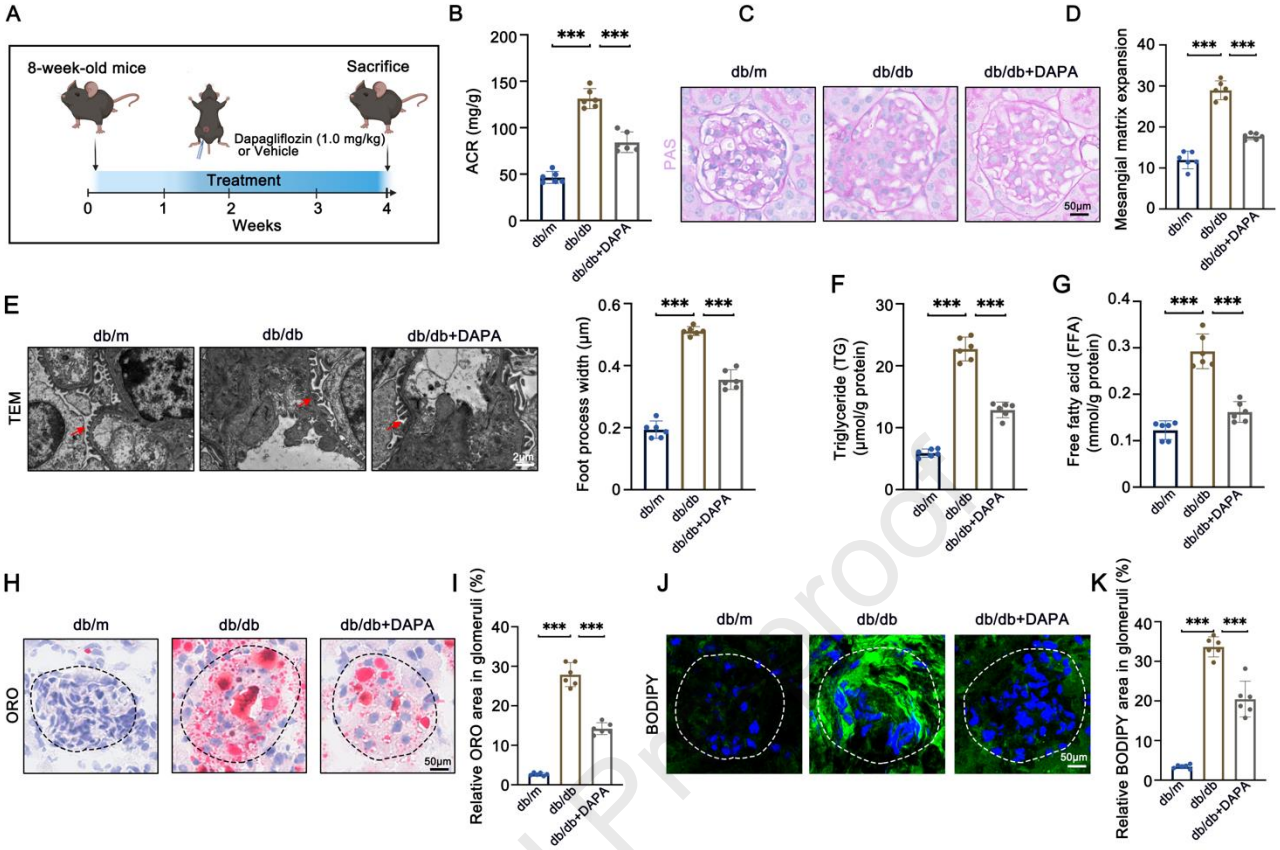

866
867

868 **Figure 2.**

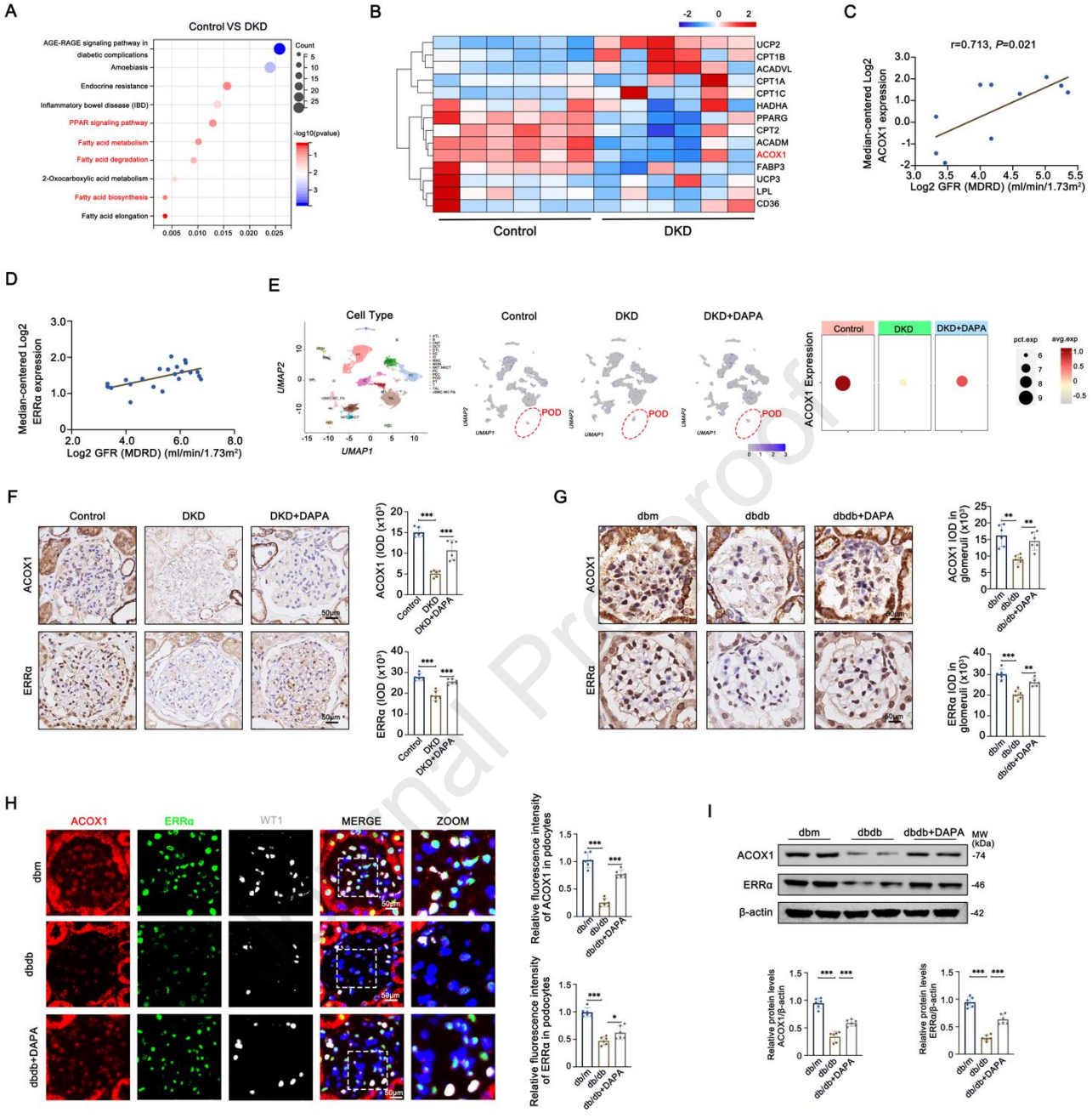

869

870

Figure 3.

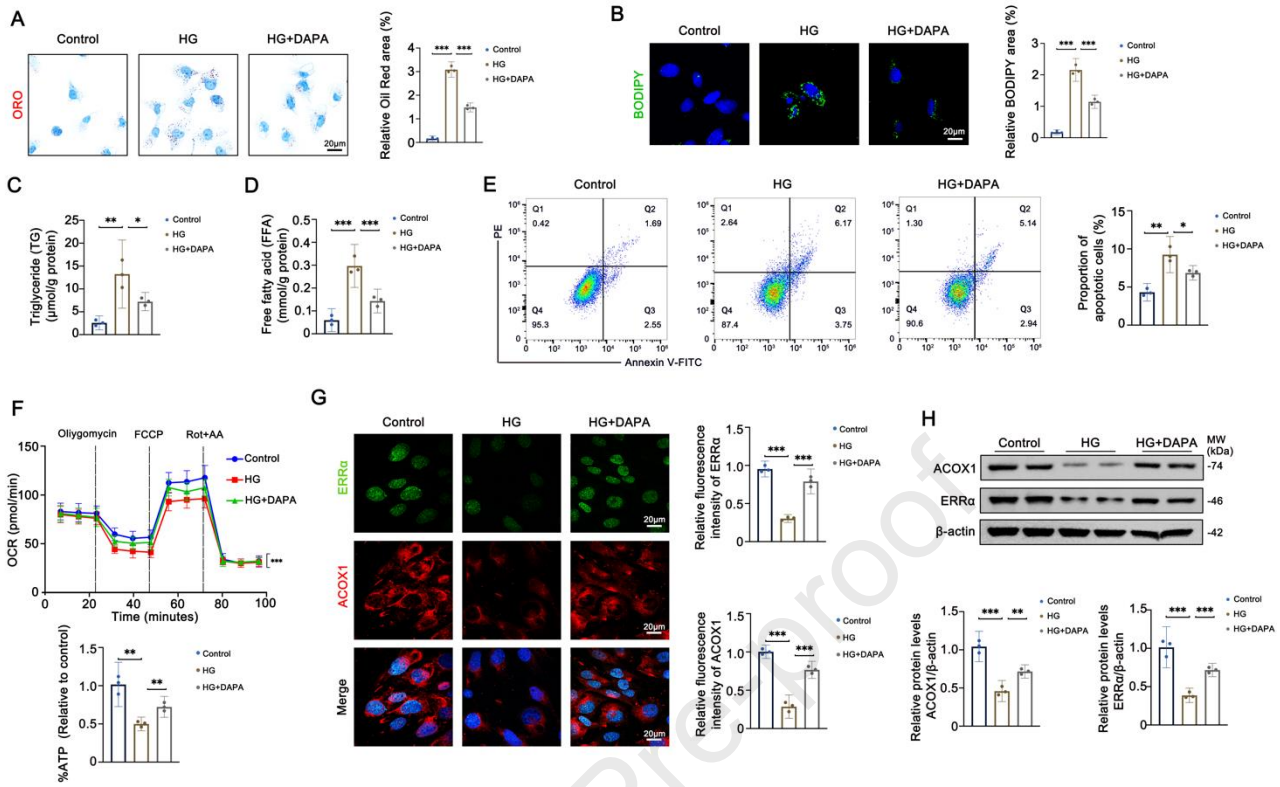

874 **Figure 4.**

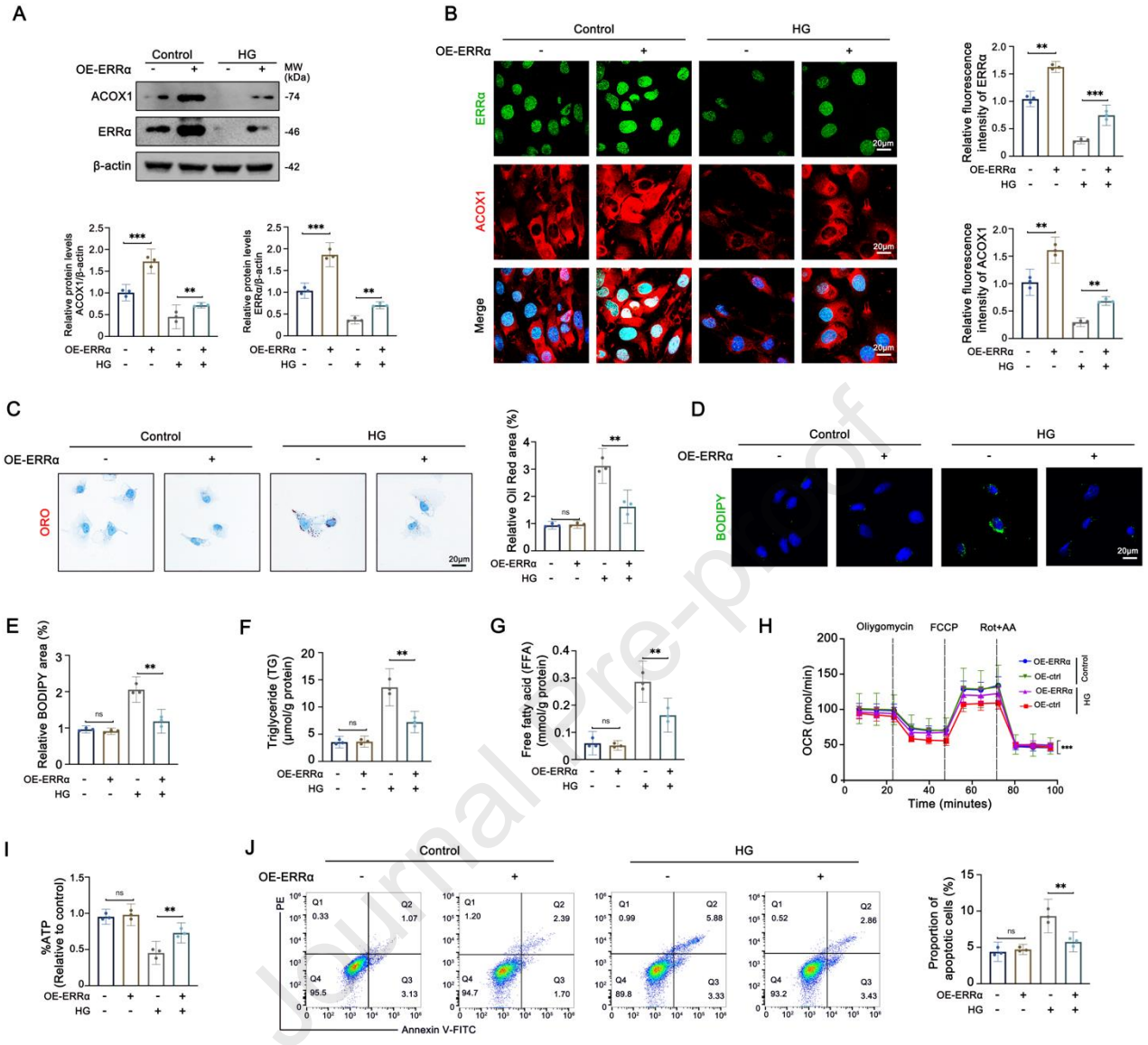

875

876

877 **Figure 5.**

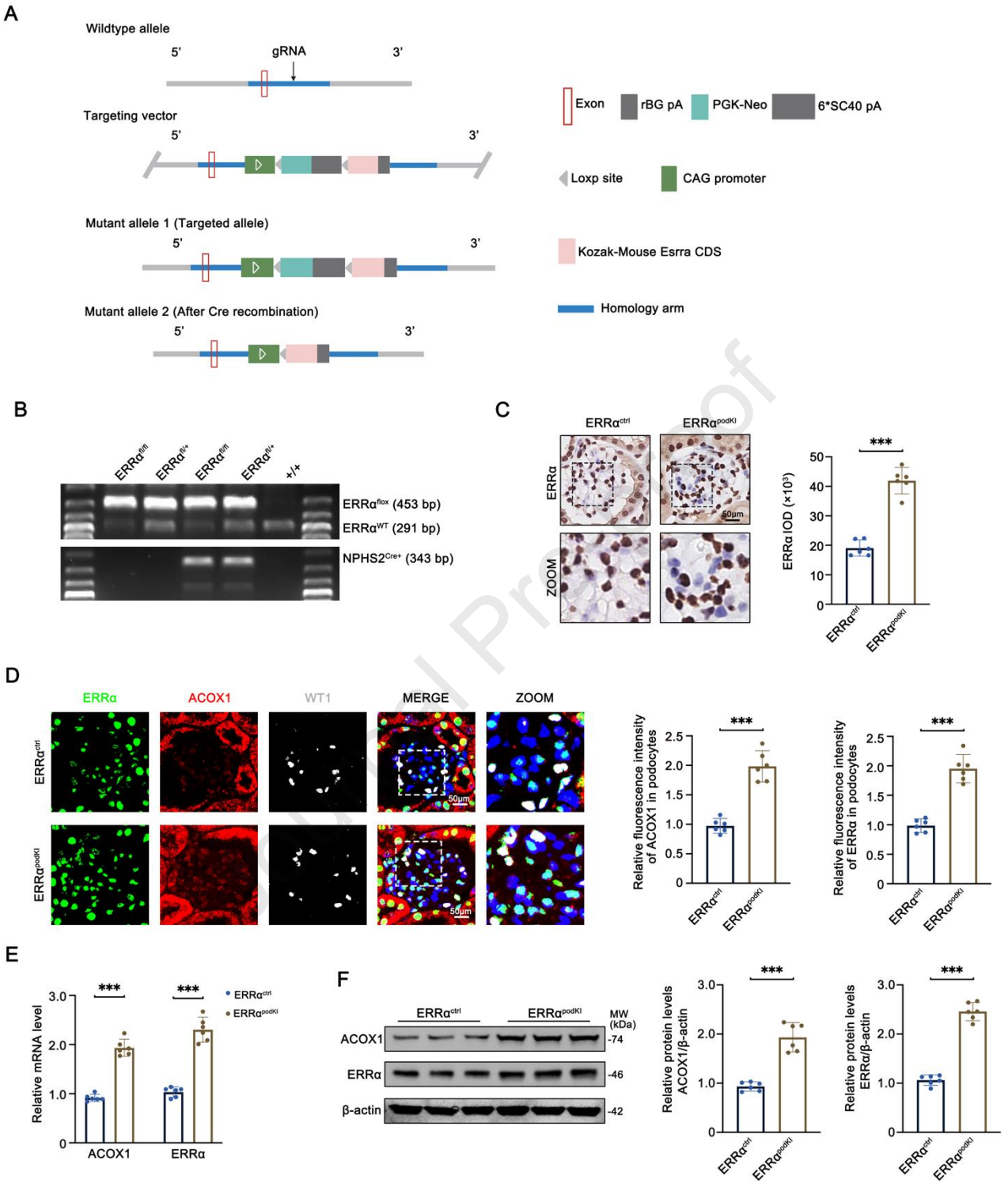

878

879

Figure 6.

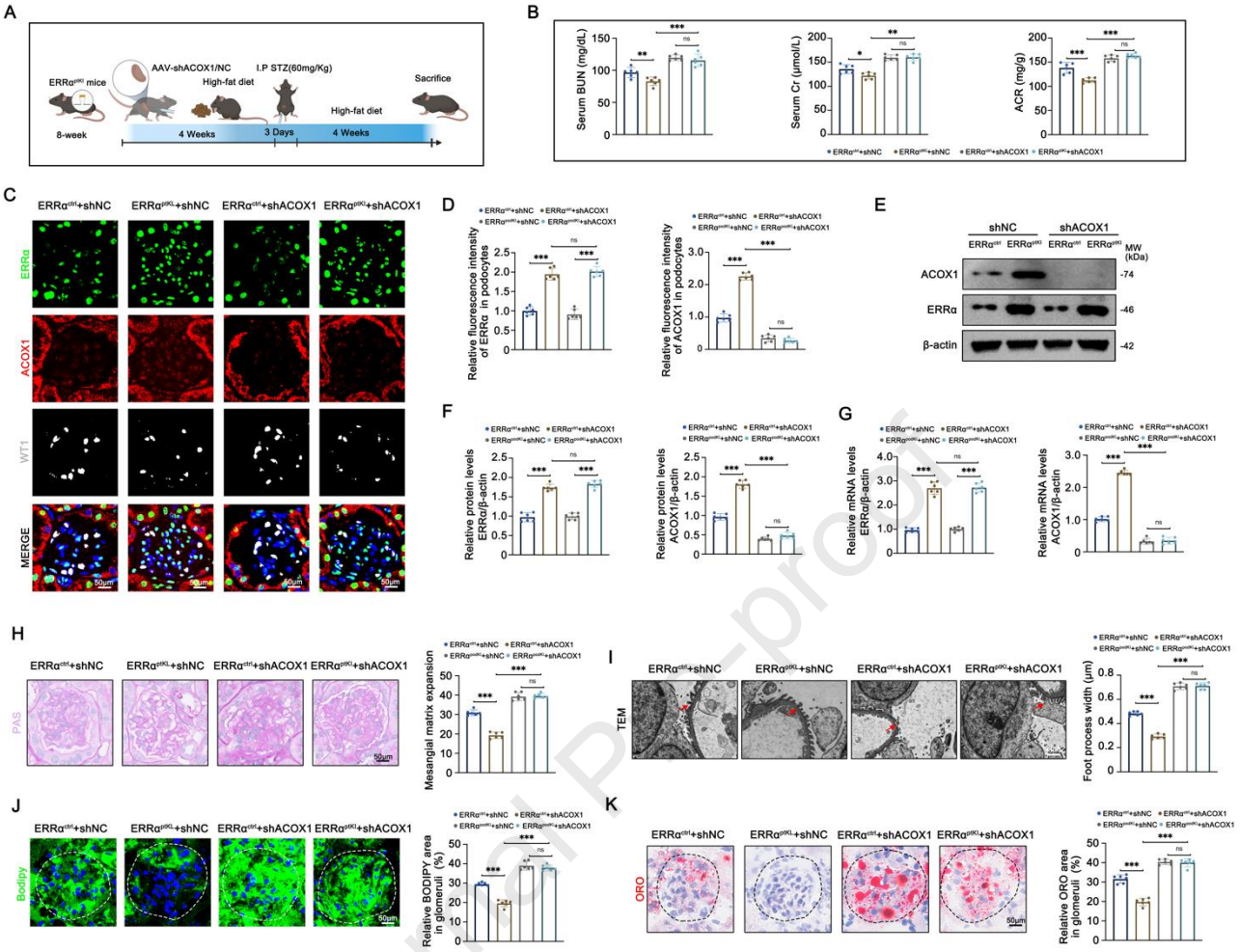

Figure 7.

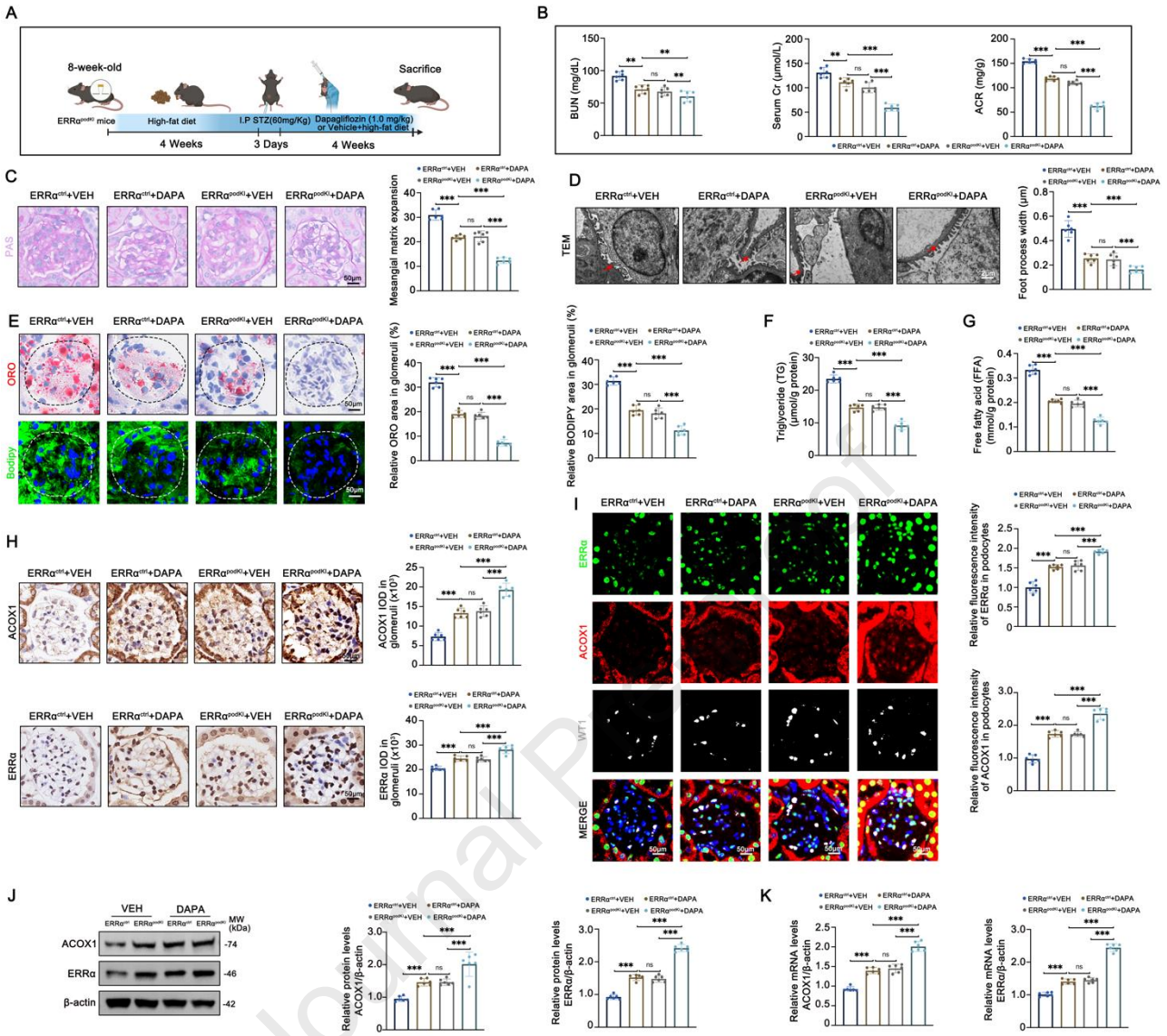

Highlights:

1. ERRα upregulation mitigates podocyte lipotoxicity.
2. ERRα/ACOX1 is crucial for podocyte FAO and OXPHOS.
3. DAPA enhances FAO through ERRα activation.
4. DAPA reduces glomerular lipid accumulation beyond glycemic control.

Declaration of interest statement

We declare that we have no financial and personal relationships with other people or organizations that can inappropriately influence our work, there is no professional or other personal interest of any nature or kind in any product, service and/or company that could be construed as influencing the position presented in, or the review of, the manuscript entitled "**Dapagliflozin Attenuates Diabetes-Induced Podocyte Lipotoxicity via ERRα-Mediated Lipid Metabolism**".